

Vector dark matter with Higgs portal in type II seesaw framework

Nandini Das,^{1,*} Tapoja Jha,^{1,2,†} and Dibyendu Nanda^{3,4,‡}

¹*School of Physical Sciences, Indian Association for the Cultivation of Science, 2A & 2B, Raja S.C. Mullick Road, Kolkata 700032, India*

²*Sodankylä Geophysical Observatory, University of Oulu, Tähteläntie, 99600 Sodankylä, Finland*

³*School of Physics, Korea Institute for Advanced Study, Seoul 02455, Republic of Korea*

⁴*Institute of Physics, Sachivalaya Marg, Bhubaneswar 751005, India*



(Received 15 February 2024; accepted 28 May 2024; published 20 June 2024)

We study the phenomenology of a vector dark matter (VDM) in a $U(1)_X$ gauged extension of the Standard Model (SM), which is set in a type II seesaw framework. When this $U(1)_X$ symmetry is spontaneously broken by the vacuum expectation value (VEV) of a newly introduced complex scalar singlet, the gauge boson Z' becomes massive. The stability of the dark matter (DM) is ensured by the presence of an exact charge conjugation symmetry resulting from the structure of the Lagrangian. On the other hand, the $SU(2)_L$ triplet scalar facilitates light neutrino masses via the type II seesaw mechanism. We have studied the phenomenology of the usual WIMP DM, considering all possible theoretical and experimental constraints that are applicable. Due to the presence of a triplet scalar, the present framework can also accommodate the observed 2σ deviation in $h \rightarrow Z\gamma$ decay rate, recently measured at the LHC. The possibility of nonthermal production of DM from the decay of the singlet scalar has also been briefly discussed.

DOI: [10.1103/PhysRevD.109.115020](https://doi.org/10.1103/PhysRevD.109.115020)

I. INTRODUCTION

The existence of a nonluminous, nonbaryonic form of matter that provides roughly 26% energy density of the Universe, popularly known as the dark matter (DM), is an undeniable fact in terms of observational evidence. Astrophysical and cosmological observational evidence, notably the study of galaxy clusters by Fritz Zwicky [1], the rotation curves of galaxy clusters by Vera Rubin [2], and the observation of bullet cluster by Chandra observatory [3] have provided compelling evidence for the existence of this mysterious species in the present Universe. Additionally, gravitational lensing and anisotropy of cosmic microwave background radiation (CMBR) measured by several cosmological experiments [4–8] have further supported the need for such enigmatic matter. The DM number density ($\Omega_{\text{DM}}h^2$) as reported by WMAP [4] and PLANCK [6] is precisely measured to be $\Omega_{\text{DM}}h^2 = 0.12 \pm 0.001$ at 68% confidence level (CL). However, the nature of DM remains a mystery. Though the observational evidence tells us about

the gravitational interaction of the DM, the particle origin of it presents an intriguing possibility. If DM is an elementary particle, it is expected to exhibit some level of interaction with the Standard Model (SM). The natural approach would be to consider the weak interaction of DM particles with the SM bath. As an interesting fact, weakly interacting massive particles (WIMPs) of electroweak mass scale can be produced thermally in the early Universe, and then they can freeze out leaving the thermal relic density close to the DM abundance of the present day. This coincidence is often noted as WIMP miracle [9].

Other than the WIMP scenario, depending on the interaction strength, DM can be a feebly interacting massive particle (FIMP) [10] or a strongly interacting massive particle (SIMP) [11,12] in nature. There are various other approaches as well namely super WIMP [13,14], secluded WIMP [15], and forbidden DM [16]. However, due to favorable detection possibilities at direct, indirect, and collider search experiments, WIMP is the most popular choice. Direct detection (DD) experiments like LUX [17], XENONnT [18,19], and PANDAX [20,21] provide stringent bounds on wide ranges of masses and couplings of WIMP. Recent bounds from the LZ experiment [22] eliminate larger DM parameter space. The WIMP scenario has been studied in various types of model setup. Depending on the choice of model, a WIMP can be a Dirac or a Majorana fermion, a scalar (pseudoscalar), or a vector boson. In comparison to fermions and scalars, vector gauge bosons as DM candidates have received a little lesser

*nandinidas.rs@gmail.com

†tapoja.jha@oulu.fi

‡dibyendu.nanda@iopb.res.in

Published by the American Physical Society under the terms of the [Creative Commons Attribution 4.0 International license](https://creativecommons.org/licenses/by/4.0/). Further distribution of this work must maintain attribution to the author(s) and the published article's title, journal citation, and DOI. Funded by SCOAP³.

attention due to the necessity of adding extra gauge extensions. Vector dark matter (VDM) has been studied in [23–28] in various gauge extensions. Specifically, VDM in $U(1)$ extension has been analyzed in [29,30]. In the above scenario, the dark matter couples to the SM through the Higgs portal via the mixing between the SM Higgs and the new scalar singlet. Here, we have discussed the variation of the VDM parameter space where the scalar sector has been extended with an additional triplet scalar. $SU(2)_L$ triplet Higgs seems to be a very obvious candidate in this context as the presence of a triplet in the scalar sector can facilitate neutrino mass, thereby solving another important question of particle physics. The neutrino mass generation will be discussed in the next paragraph. The presence of the extra triplet will provide extra annihilation channels for the dark matter; thus, it has more control in tuning of the relic abundance.

Neutrino mass is one of the most compelling reasons to go beyond the Standard Model (BSM). Neutrino oscillation data from various experiments confirmed that neutrinos have tiny mass $\sim \mathcal{O}(0.1)$ eV [31,32]. The most popular way to generate such tiny neutrino mass at tree level is the seesaw mechanism. Based on the particle contents of the model, there are three types of seesaw mechanisms. Type I seesaw [33–36] extends the SM particle spectrum by three heavy right-handed neutrinos, whereas type II [37–43] adds a $SU(2)_L$ triplet scalar, and type III [44–47] adds a $SU(2)_L$ triplet fermion. Type I seesaw models with an extra $U(1)_X$ symmetry have been studied in Ref. [48–50] in the context of dark matter phenomenology. Interestingly, in addition to the added advantage of vacuum stability, the type II seesaw mechanism can generate small neutrino masses with a $SU(2)_L$ triplet scalar with a very small vacuum expectation value (VEV) v_t , whereas the type I seesaw mechanism requires three right-handed Majorana neutrinos with masses in the range 10^9 – 10^{10} GeV. Moreover, if we choose the triplet VEV v_t to be in the range 1–3 GeV ($> 10^{-4}$ GeV), we can get a mass range for the doubly charged and singly charged scalar that can be probed at colliders [51]. Fermionic DM with type II seesaw in $U(1)_X$ model has been discussed in [52,53].

In this article, we explore the possibility of the existence of a gauge boson VDM in a general gauged $U(1)_X$ extension of SM where neutrino mass is generated by the type II seesaw mechanism. In addition to a triplet scalar, a $SU(2)_L$ singlet, the only particle that carries the $U(1)_X$ charge, is necessary to break this symmetry spontaneously resulting in a massive vector boson, Z' , which plays the role of DM in this model. The stability of DM is ensured by an exact charge conjugation symmetry, which arises due to $U(1)_X$ invariance. The interaction of the singlet scalar with the SM Higgs doublet acts as a portal between the dark sector and the visible sector. Moreover, the presence of a triplet scalar in this scenario gives rise to interesting DM phenomenology by mixing with the SM Higgs doublet and

the scalar singlet and finally resulting into an enhanced DM parameter space. Therefore, we study an interesting scenario that addresses the nonzero neutrino mass and DM abundance in a unified framework. Another interesting factor that prompts us to explore this scenario is the recent combined report by the ATLAS and CMS Collaborations on the $h \rightarrow Z\gamma$ decay channel. Their findings reveal a combined signal strength $\mu_{Z\gamma} = 2.2 \pm 0.7$ [54], indicating a slight 2σ discrepancy compared to the Standard Model prediction of $\mu_{Z\gamma} = 1$. Some recent studies [55,56] show a way to accommodate such excess by different model perspectives. Type II seesaw triplet (the singly charged and doubly charged component) can also accommodate nonstandard values of $\mu_{Z\gamma}$ as shown in various studies [57,58]. We show that in addition to the dominant contribution of the triplet charged scalar components, the new couplings introduced by the complex scalar singlet can affect the signal strengths $\mu_{\gamma\gamma}$ and $\mu_{Z\gamma}$.

This article is organized as follows. In Sec. II, we describe the model in detail along with the generation of neutrino mass by the type II seesaw mechanism. In Sec. III, the experimental and theoretical constraints on the model parameters are discussed. In Sec. IV, we finally discuss the phenomenology of the thermal VDM with the prediction of possible experimental signature of this allowed model parameter space from DD. In Sec. V, the possibility of the freeze-in scenario of the VDM is discussed briefly. Finally, the conclusion is drawn in Sec. VI.

II. BASIC FRAMEWORK

Let us now introduce the detailed framework of this model. We are exploring an extension of the SM that involves an additional triplet (Δ) to the scalar sector to facilitate the generation of neutrino mass through the type-II seesaw mechanism via a lepton number nonconserving interaction. Furthermore, a complex scalar singlet (S) has been introduced that is charged under an additional abelian $U(1)_X$ gauge symmetry. When S acquires VEV (v_s), it spontaneously breaks $U(1)_X$ symmetry and makes the gauge boson (Z') massive, which serves as a potential DM candidate of the universe in this model. The total Lagrangian of the model is given by

$$\mathcal{L}_{\text{Tot}} = \mathcal{L}_{\text{SM}} + \mathcal{L}_{\text{Scalar}} + \mathcal{L}_{Z'_{\text{Dark}}} + \mathcal{L}_{Y_{\text{uk}}}^{\Delta}, \quad (1)$$

where, \mathcal{L}_{SM} represents the SM Lagrangian without the scalar sector. The different BSM interaction terms are analyzed in detail in the following sections.

A. Scalar sector

The most general renormalizable Lagrangian involving a triplet, a singlet scalar along with the SM Higgs doublet can be written as

$$\mathcal{L}_{\text{Scalar}} = \mathcal{L}_{\text{Scalar}}^{\text{Kin}} - V(\Phi, \Delta, S), \quad (2)$$

$$D_\mu S = \partial_\mu S + ig_x x_s Z'_\mu S. \quad (6)$$

where the kinetic part of scalar fields is given by

$$\mathcal{L}_{\text{Scalar}}^{\text{Kin}} = (D^\mu \Phi)^\dagger (D_\mu \Phi) + \text{Tr}[(D^\mu \Delta)^\dagger (D_\mu \Delta)] + (D^\mu S)^* (D_\mu S), \quad (3)$$

where

$$D_\mu \Phi = \partial_\mu \Phi + \frac{ig}{2} W_\mu^a \sigma^a \Phi + \frac{ig'}{2} B_\mu \Phi, \quad (4)$$

$$D_\mu \Delta = \partial_\mu \Delta + \frac{ig}{2} [W_\mu^a \sigma^a, \Delta] + ig' B_\mu \Delta, \quad (5)$$

Here, g_x is the gauge coupling of $U(1)_X$, and x_s is the $U(1)_X$ charge of complex scalar singlet S that is taken to be unity for the whole analysis. The covariant derivative of S takes an important role in the DM dynamics and has been discussed in the dark sector. The expressions of the SM Higgs doublet Φ , the scalar triplet Δ , and the S are given by

$$\Phi = \begin{pmatrix} \phi^+ \\ \phi^0 \end{pmatrix}, \quad \Delta = \begin{pmatrix} \frac{\Delta^+}{\sqrt{2}} & \Delta^{++} \\ \Delta^0 & -\frac{\Delta^+}{\sqrt{2}} \end{pmatrix}, \quad S = (S_r + i s_i). \quad (7)$$

The scalar potential is given by

$$\begin{aligned} V(\Phi, \Delta, S) = & \mu_\Phi^2 (\Phi^\dagger \Phi) + \lambda (\Phi^\dagger \Phi)^2 + M_\Delta^2 \text{Tr}[\Delta^\dagger \Delta] + \lambda_1 (\Phi^\dagger \Phi) \text{Tr}[\Delta^\dagger \Delta] \\ & + \lambda_2 (\text{Tr}[\Delta^\dagger \Delta])^2 + \lambda_3 \text{Tr}[(\Delta^\dagger \Delta)^2] + \lambda_4 (\Phi^\dagger \Delta \Delta^\dagger \Phi) + [\mu \Phi^T i \sigma_2 \Delta^\dagger \Phi + \text{H.c.}] \\ & + \mu_s^2 (S^\dagger S) + \lambda_s (S^\dagger S)^2 + \lambda_{s\phi} (S^\dagger S) (\Phi^\dagger \Phi) + \lambda_{s\Delta} (S^\dagger S) \text{Tr}[\Delta^\dagger \Delta]. \end{aligned} \quad (8)$$

After electroweak symmetry breaking (EWSB), the scalars can be expanded around VEV as

$$\phi^0 = \frac{1}{\sqrt{2}}(v_d + h_0 + i g_0), \quad \Delta_0 = \frac{1}{\sqrt{2}}(v_t + \delta_0 + i \eta_0), \quad S = \frac{1}{\sqrt{2}}(v_s + s_r + i s_i). \quad (9)$$

The scalar kinetic terms of Eq. (3) give rise to the masses of W^\pm , Z_μ , and Z'_μ after symmetry breaking as the following:

$$m_W^2 = \frac{1}{4} g^2 (v_d^2 + 2v_t^2), \quad m_Z^2 = \frac{1}{4} \frac{g^2}{\cos^2 \theta_W} (v_d^2 + 4v_t^2), \quad M_{Z'}^2 = g_x^2 v_s^2, \quad (10)$$

where θ_W is the Weinberg angle. The triplet VEV (v_t) gives an additional contribution to both the W^\pm mass and Z boson mass and in turn contributes to the ρ parameter (discussed in Sec. III). The minimization of the scalar potential yields the following relations:

$$\mu_\Phi^2 = -\left(v_d^2 \lambda + \frac{v_t^2}{2} (\lambda_1 + \lambda_4) + \frac{v_s^2}{2} \lambda_{s\phi} - \sqrt{2} v_t \mu \right), \quad (11)$$

$$M_\Delta^2 = -\left(\frac{v_d^2}{2} (\lambda_1 + \lambda_4) + v_t^2 (\lambda_2 + \lambda_3) + \frac{v_s^2}{2} \lambda_{s\Delta} - \frac{v_d^2 \mu}{\sqrt{2} v_t} \right), \quad (12)$$

$$\mu_s^2 = -\frac{1}{2} (v_d^2 \lambda_{s\phi} + v_t^2 \lambda_{s\Delta}) - v_s^2 \lambda_s. \quad (13)$$

Using the above minimization conditions, the mass squared of the doubly charged states $\Delta^{\pm\pm}$ is given by

$$m_{H^{\pm\pm}}^2 = \frac{v_d^2 \mu}{\sqrt{2} v_t} - \frac{v_d^2 \lambda_4}{2} - v_t^2 \lambda_3. \quad (14)$$

The charged scalar mass matrix in the basis of (ϕ^\pm, Δ^\pm) is noted as

$$\mathcal{M}_C^2 = \begin{pmatrix} -\frac{v_t^2 \lambda_4}{2} + \sqrt{2} v_t \mu & \frac{v_d}{4} (\sqrt{2} v_t \lambda_4 - 4\mu) \\ \frac{v_d}{4} (\sqrt{2} v_t \lambda_4 - 4\mu) & -\frac{v_d^2}{4 v_t} (v_t \lambda_4 - 2\sqrt{2} \mu) \end{pmatrix}. \quad (15)$$

The mass eigenstates (G^\pm, H^\pm) in terms of the gauge eigenstates can be written as

$$\begin{pmatrix} G^\pm \\ H^\pm \end{pmatrix} = \begin{pmatrix} \cos \theta & \sin \theta \\ -\sin \theta & \cos \theta \end{pmatrix} \begin{pmatrix} \phi^\pm \\ \Delta^\pm \end{pmatrix}, \quad (16)$$

where θ is the mixing angle and reads as

$$\tan \theta = \frac{\sqrt{2} v_t}{v_d}. \quad (17)$$

The charged Goldstone gives mass to W^\pm . The mass eigenvalue of the physical scalar H^\pm is as follows:

$$m_{H^\pm}^2 = \frac{v_d^2 + 2v_t^2}{4v_t} (2\sqrt{2}\mu - v_t\lambda_4). \quad (18)$$

The CP odd mass matrix in the basis of (g_0, η_0) is given by

$$\mathcal{M}_A^2 = \begin{pmatrix} 2\sqrt{2}v_t\mu & -\sqrt{2}v_d\mu \\ -\sqrt{2}v_d\mu & \frac{v_d^2\mu}{\sqrt{2}v_t} \end{pmatrix}, \quad (19)$$

where the off-diagonal entry arises from the lepton number violating term of the scalar potential and introduces mixing among the states. This matrix can be diagonalized by a rotation of the states by an orthogonal matrix. The mass eigenstates can be expressed as

$$\begin{pmatrix} \zeta \\ A \end{pmatrix} = \begin{pmatrix} \cos\beta & \sin\beta \\ -\sin\beta & \cos\beta \end{pmatrix} \begin{pmatrix} g_0 \\ \eta_0 \end{pmatrix}, \quad (20)$$

where β is the mixing angle and is given by

$$\tan\beta = \frac{2v_t}{v_d}. \quad (21)$$

Here, ζ is the Goldstone mode, which eventually makes the Z boson massive. A is the physical CP odd Higgs with mass eigenvalue,

$$m_A = \sqrt{\frac{v_d^2 + 4v_t^2}{2} \mu}. \quad (22)$$

The CP even mass matrix in the basis of (h_0, δ_0, s_r) is given by

$$\mathcal{M}_E^2 = \begin{pmatrix} 2v_d^2\lambda & v_d v_t \left(-\frac{4m_{H^\pm}^2}{v_d^2 + 2v_t^2} + \frac{2m_A^2}{v_d^2 + 4v_t^2} + \lambda_1 \right) & v_d v_s \lambda_{s\phi} \\ v_d v_t \left(-\frac{4m_{H^\pm}^2}{v_d^2 + 2v_t^2} + \frac{2m_A^2}{v_d^2 + 4v_t^2} + \lambda_1 \right) & -2m_{H^{\pm\pm}}^2 + v_d^2 \left(\frac{4m_{H^\pm}^2}{v_d^2 + 2v_t^2} - \frac{m_A^2}{v_d^2 + 4v_t^2} \right) + 2v_t^2\lambda_2 & v_s v_t \lambda_{s\Delta} \\ v_d v_s \lambda_{s\phi} & v_s v_t \lambda_{s\Delta} & 2v_s^2\lambda_s \end{pmatrix}. \quad (23)$$

Gauge basis to mass basis transformation can be obtained by

$$\begin{pmatrix} h \\ H_1 \\ H_2 \end{pmatrix} = \mathcal{O}_\alpha \begin{pmatrix} h_0 \\ \delta_0 \\ s_r \end{pmatrix}, \quad \text{where } \mathcal{O}_\alpha = R_3 \cdot R_2 \cdot R_1, \quad (24)$$

with

$$R_1 = \begin{pmatrix} \cos\alpha_1 & \sin\alpha_1 & 0 \\ -\sin\alpha_1 & \cos\alpha_1 & 0 \\ 0 & 0 & 1 \end{pmatrix}, \quad R_2 = \begin{pmatrix} \cos\alpha_2 & 0 & \sin\alpha_2 \\ 0 & 1 & 0 \\ -\sin\alpha_2 & 0 & \cos\alpha_2 \end{pmatrix}, \quad R_3 = \begin{pmatrix} 1 & 0 & 0 \\ 0 & \cos\alpha_3 & \sin\alpha_3 \\ 0 & -\sin\alpha_3 & \cos\alpha_3 \end{pmatrix}. \quad (25)$$

Here, (h, H_1, H_2) are the mass eigenstates. The gauge eigenstates in terms of mass eigenstates can be expressed as

$$h_0 = c_{\alpha_1} c_{\alpha_2} h - (c_{\alpha_3} s_{\alpha_1} + c_{\alpha_1} s_{\alpha_2} s_{\alpha_3}) H_1 + (s_{\alpha_1} s_{\alpha_3} - c_{\alpha_1} c_{\alpha_3} s_{\alpha_2}) H_2, \quad (26)$$

$$\delta_0 = c_{\alpha_2} s_{\alpha_1} h + (c_{\alpha_1} c_{\alpha_3} - s_{\alpha_1} s_{\alpha_2} s_{\alpha_3}) H_1 - (c_{\alpha_3} s_{\alpha_1} s_{\alpha_2} + c_{\alpha_1} s_{\alpha_3}) H_2, \quad (27)$$

$$s_r = s_{\alpha_2} h + c_{\alpha_2} s_{\alpha_3} H_1 + c_{\alpha_2} c_{\alpha_3} H_2. \quad (28)$$

In the above equations, s_{α_i} and c_{α_i} where $i = 1, 2, 3$, stand for $\sin\alpha_i$ and $\cos\alpha_i$, respectively. Scalar potential param-

eters (λ s) can be expressed in terms of the physical masses of the scalars, mixing angles, and VEVs. Such relations, listed in Appendix A 1, help us to parametrize the model in terms of physical quantities. So, the set of free parameters of this model is $\{\sin\alpha_1, \sin\alpha_2, \sin\alpha_3, m_{H_1}, m_{H_2}, m_A, m_{H^{\pm\pm}}, m_{H^\pm}, v_s\}$. We will later see that the triplet scalar masses would be almost degenerate from theoretical constraints. So, the set of free parameters are

$$\{\sin\alpha_1, \sin\alpha_2, \sin\alpha_3, m_\Delta, m_S, v_s\},$$

where m_Δ represents masses of the scalars $m_{H^{\pm\pm}}, m_{H^\pm}, m_{H_1}, m_A$, which have large triplet component

in them, and m_S is the mass of scalar H_2 , which is dominantly singlet.

B. Dark sector

Now let us discuss the role of the additional gauge boson, which plays the role of DM in our framework. Apart from the singlet scalar S , no other fields couple to this extra gauge boson Z' . When the singlet scalar S acquires a VEV after the spontaneous breaking of $U(1)_X$, Z' becomes massive. The mass of the DM is given by

$$M_{Z'} = g_X v_s.$$

We can choose either g_X or v_s to be a free parameter. For the constraints coming from the scalar sector, we would be using v_s , whereas in the DM phenomenology, we will translate the limit of v_s in g_X vs $M_{Z'}$ plane.

The $U(1)_X$ invariant Lagrangian enjoys an additional dark conjugation symmetry [24,59] described as

$$\begin{aligned} Z_2^{(A)} : Z'_\mu &\rightarrow -Z'_\mu, & S &\rightarrow S^*, \\ Z_2^{(B)} : Z'_\mu &\rightarrow -Z'_\mu, & S &\rightarrow -S^*. \end{aligned}$$

If we consider this symmetry to be exact, the kinetic mixing between the Z' and B field [$U(1)_Y$ gauge boson of the SM] is prohibited consequently. If we relax the symmetry and allow a gauge kinetic mixing term proportional to $Z'_{\mu\nu} B^{\mu\nu}$ along with the canonical kinetic term for Z'_μ in $\mathcal{L}_{Z'_{\text{Dark}}}$, the kinetic mixing angle needs to be very small to make the Z' a viable decaying DM candidate. Nevertheless, we disregard that scenario and consider the dark charge conjugation symmetry to be exact in this framework. All SM fields along with the extra scalar triplet do not carry any $U(1)_X$ charge; hence, they do not couple to the extra gauge boson. This ensures the stability of this new heavy gauge boson Z' , rendering it a viable DM candidate in this scenario.

C. Yukawa Lagrangian and neutrino mass

In the present framework, the SM Yukawa Lagrangian is augmented by a seesaw mass term involving the Higgs triplet and two lepton doublets as follows:

$$\mathcal{L}_{\text{Yuk}}^\Delta = -(Y_\Delta)_{jk} L_j^T C i \sigma_2 \Delta L_k + \text{H.c.}, \quad (29)$$

where Y_Δ is the 3×3 Yukawa matrix, C is the charge conjugation matrix, and L is SM lepton doublet. The following Majorana mass for neutrinos can be generated from the above Yukawa term,

$$m_\nu = \sqrt{2} Y_\Delta v_t. \quad (30)$$

Since $v_t \sim \mathcal{O}(\text{GeV})$ in our analysis and the neutrino mass scale is in the eV range, therefore, Y_Δ must be very small.

For neutrino mass scale $m_\nu \sim 0.8$ eV and $v_t \sim 1$ GeV, $Y_\Delta \sim 5.66 \times 10^{-10}$. Apart from the kinematics, the value of Y_Δ controls the decay mode of $H^{\pm\pm}$. The partial decay width of $H^{\pm\pm}$ to like-sign dileptons being proportional to $|Y_\Delta|^2$, $H^{\pm\pm} \rightarrow \ell^\pm \ell^\pm$ would be highly suppressed for our choice of v_t , which corresponds to very small Y_Δ , and the $H^{\pm\pm} \rightarrow W^\pm W^\pm$ channel will dominate consequently.

III. THEORETICAL AND EXPERIMENTAL CONSTRAINTS ON MODEL PARAMETERS

Now we are ready to discuss the possible experimental and theoretical constraints on the parameters of this model that would be used in our analysis.

A. Experimental constraints

- (i) *ρ parameter constraint*: The triplet vacuum expectation value v_t contributes to the W^\pm and Z boson masses at the tree level [see Eq. (10)], thus affecting the value of the ρ parameter, which is defined in terms of the VEVs v_d and v_t of the SM doublet and triplet scalars, respectively, as

$$\rho = \frac{m_W^2}{m_Z^2 c_W^2} = \frac{1 + \frac{2v_t^2}{v_d^2}}{1 + \frac{4v_t^2}{v_d^2}}. \quad (31)$$

The electroweak precision data constrains the ρ parameter to be very close to its SM value. From the latest data, it is constrained as $\rho = 1.00038 \pm 0.00020$ [31], which signifies that at 3σ level, v_t should be $\lesssim 2.6$ GeV.

- (ii) *Experimental limits on singly and doubly charged scalar masses*: This scenario predicts a plethora of heavy scalars that have been extensively searched at both e^+e^- and hadron colliders. The negative search results at LEP-2 put a limit on the singly charged mass $m_{H^\pm} > 78$ (GeV) [60]. On the other hand, the lower limit on the doubly charged scalar mass $m_{H^{\pm\pm}}$ from the LHC is highly model dependent. The decay modes of the $H^{\pm\pm}$ depend on v_t and the mass splitting $m_{H^{\pm\pm}} - m_{H^\pm}$. For $v_t < 10^{-4}$ GeV (large Yukawa coupling) and assuming degenerate scalars, $H^{\pm\pm}$ decays to like-signed dilepton with almost 100% probability. The decay mode of $H^{\pm\pm}$ changes rather drastically when $v_t > 10^{-4}$ GeV, leading to various competing channels, like $H^\pm H^\mp$, $W^\pm W^\mp$, and $W^\pm H^\mp$, if kinematically allowed. From current analysis at the LHC, $m_{H^{\pm\pm}} \gtrsim 1080$ GeV [61] is allowed for $H^{\pm\pm} \rightarrow \ell^\pm \ell^\pm$ decay where the branching ratios to each of the possible leptonic final states ($ee, \mu\mu, \tau\tau, e\mu, e\tau, \mu\tau$) are considered to be equal. However in a type II seesaw framework, when $H^{\pm\pm} \rightarrow W^\pm W^\pm$ decay is allowed, doubly charged

Higgs mass has a lower bound of 420 GeV [51]. In the following analysis, we have chosen $v_i \sim \mathcal{O}(1 \text{ GeV})$ and $m_{H^{\pm\pm}}$ to be greater than 420 GeV.

- (iii) *Collider constraints on the neutral scalar masses and mixing:* The Higgs decay width measurement at LHC can constrain the mixing angle between the triplet and SM doublet. The upper bound on this mixing angle $\sin \alpha_1$ is $\lesssim 0.05$ [62], which is consistent with the experimental observation of the $h \rightarrow WW^*$ branching ratio. A similar bound is obtained on the mixing angle of the complex scalar singlet with SM Higgs from theoretical and experimental constraints. The most stringent bound comes from W mass correction at NLO [63]. For m_S in the range $\sim \{200-1000\}$ GeV, the upper bound on the mixing angle $\sin \alpha_2$ varies between (0.2–0.3) [64]. In this model, the value of $\sin \alpha_1$ is taken to be < 0.05 , and the maximum value of $\sin \alpha_2$ is taken to be 0.1.
- (iv) *Constraint from lepton flavor violation:* The Higgs triplet in the model induces lepton flavor violating (LFV) decays at tree level. The branching ratio (BR) of the process $\ell_i \rightarrow \ell_j \ell_k \ell_m$ mediated by a doubly charged scalar is given by

$$\text{BR}(\ell_i \rightarrow \bar{\ell}_j \ell_k \ell_m) = \frac{|(Y_\Delta)_{ij}(Y_\Delta)_{km}|^2}{64G_F^2 m_{H^{\pm\pm}}^4}. \quad (32)$$

Among all possible combinations from the above-mentioned branching ratios, the most stringent bound comes from $\mu \rightarrow eee$ with $\text{BR}(\mu \rightarrow eee) \lesssim 1.0 \times 10^{-12}$ from SINDRUM experiment [65]. As Yukawa parameters are inversely proportional to v_i , we can extract a lower limit on v_i from the above expression for a particular mass of $H^{\pm\pm}$. Another lepton flavor violating process, namely $\ell_i \rightarrow \ell_j \gamma$, receives nonstandard contribution via loop diagrams of charged (singly and doubly) scalars. The BR of $\mu \rightarrow e\gamma$ gives the most stringent bound among these decays, and the corresponding expression is given by [52]

$$\text{BR}(\mu \rightarrow e\gamma) = \frac{48\pi^3 \alpha_{em}}{G_F^2 m_{H^{\pm\pm}}^2} \left| (Y_\Delta^\dagger Y_\Delta)_{e\mu} \frac{1}{16\pi^2} \frac{3}{16} \right|^2. \quad (33)$$

The latest bound on $\text{BR}(\mu \rightarrow e\gamma)$ ($\lesssim 4.2 \times 10^{-13}$) has been recently reported by MEG collaboration [66].

In this model, Y_Δ being very small as mentioned before [see under Eq. (30)], the branching ratios of the aforementioned processes are way smaller than the reported experimental bounds.

- (v) *Constraint from oblique parameters:* Dominant contribution in oblique parameters comes from the charged Higgs sector of the triplet scalar. The most stringent bound comes from the T parameter, and it demands the mass splitting of the doubly charged and the singly charged scalars to be $\lesssim 40$ GeV [67]. Our DM sector constraints are insensitive to this mass splitting, so the triplet scalar masses are taken to be degenerate for the analysis of the DM part.
- (vi) *Higgs invisible decay constraint:* Current Higgs searches at the LHC put stringent limits on the branching fraction of Higgs invisible decay. In our scenario, SM Higgs can decay to a pair of VDM through mixing with the singlet scalar when $m_h > 2M_{Z'}$. The expression of Higgs invisible branching ratio is given by

$$\text{BR}(h \rightarrow \text{invisible}) = \frac{\Gamma(h \rightarrow Z'Z')}{\Gamma(h \rightarrow Z'Z') + \Gamma(h \rightarrow \text{SMSM})}. \quad (34)$$

This ratio is constrained to be $\leq 10.5\%$ by ATLAS Collaboration [68]. Here, for $M_{Z'} < 62.5$ GeV, the coupling of Higgs to DM will be constrained by this condition.

- (vii) *Constraints from $h \rightarrow \gamma\gamma$ and $h \rightarrow Z\gamma$:* In the SM, due to the absence of tree level coupling, $h \rightarrow \gamma\gamma$ takes place at one loop level via the exchange of charged fermions and W^\pm bosons. This particular decay mode plays a significant role in the discovery of the SM Higgs at the LHC. Being a loop-mediated process, it shows high sensitivity to any new particles that couple to both the SM Higgs and the photon. Therefore, in the type II seesaw model, the existence of new heavy H^\pm and $H^{\pm\pm}$ scalars has the potential to supplement the contributions to this particular channel. The impact of this additional contribution on the $\Gamma(h \rightarrow \gamma\gamma)$ can vary, either enhancing or reducing it, depending on the specific model parameters. The partial decay width with these spin-0, spin-1/2, spin-1 contribution is given by [58,69–72]

$$\Gamma(h \rightarrow \gamma\gamma) = \frac{\alpha^2 G_F m_h^3}{128\sqrt{2}\pi^3} \left| \sum_f N_c Q_f^2 g_{hf\bar{f}} A_{1/2}^h(\tau_f) + g_{hW^+W^-} A_1^h(\tau_W) + \tilde{g}_{hH^\pm H^\mp} A_0^h(\tau_{H^\pm}) + 4\tilde{g}_{hH^{\pm\pm} H^{\mp\mp}} A_0^h(\tau_{H^{\pm\pm}}) \right|^2, \quad (35)$$

where α is the fine structure constant, G_F is the Fermi coupling constant, and N_c and Q_f are the color factor and the electric charge of the fermion in the loop, respectively. $\tau_i = \frac{m_h^2}{4m_i^2}$, where i corresponds to the virtual particles in the loop

($f, W, H^\pm, H^{\pm\pm}$ here). The expression of the couplings ($g_{hW^+W^-}$ etc.) and loop functions [$A_i^h(\tau_j)$ etc.] are given in the Appendix A 2.

The first two terms on the right-hand side denote the SM fermions and W boson contribution in the loop, whereas the last two terms represent the nonstandard contribution coming from the singly charged (H^\pm) and the doubly charged ($H^{\pm\pm}$) scalars. Except for the coupling and mass dependence, the $H^{\pm\pm}$ term has a relative factor of four with respect to the H^\pm term in the amplitude due to its enhanced charge.

Similarly, the partial decay width of $h \rightarrow Z\gamma$ is given by [57,73]

$$\Gamma(h \rightarrow Z\gamma) = \frac{\alpha G_F^2 m_W^2 m_h^3}{64\pi^2} \left(1 - \frac{m_Z^2}{m_h^2}\right)^3 \left| \frac{1}{c_W} \sum_f N_c Q_f (2I_3^f - 4Q_f s_W^2) g_{hf\bar{f}} A_{1/2}^h(\tau_h^f, \tau_Z^f) \right. \\ \left. + c_W g_{hW^+W^-} A_1^h(\tau_h^W, \tau_Z^W) + \frac{1}{s_W} g_{ZH^\pm H^\mp} \tilde{g}_{hH^\pm H^\mp} A_0^h(\tau_h^{H^\pm}, \tau_Z^{H^\pm}) + \frac{2}{s_W} g_{ZH^{\pm\pm} H^{\mp\mp}} \tilde{g}_{hH^{\pm\pm} H^{\mp\mp}} A_0^h(\tau_h^{H^{\pm\pm}}, \tau_Z^{H^{\pm\pm}}) \right|^2, \quad (36)$$

where $\tau_j^i = \frac{4m_i^2}{m_j^2}$, with $i = f, W, H^\pm, H^{\pm\pm}$ and $j = h, Z$. The necessary couplings and loop functions are mentioned in Appendix A 2.

The partial decay width of $h \rightarrow \gamma\gamma$ and $h \rightarrow Z\gamma$ in the type II seesaw extended model differs from SM due to the presence of a triplet scalar. In SM, the W loop interferes with the top loop destructively. In the presence of triplet scalars, the doubly charged and singly charged scalars interfere constructively with the W contribution; as a result, the decay width enhances. The effect of triplet scalar in the $h \rightarrow \gamma\gamma$ and $h \rightarrow Z\gamma$ signal has been discussed in Ref. [57,58]. Here, as another CP even scalar from the complex scalar singlet mixes with the Higgs, the coupling of Higgs to the charged scalars is modified with $\lambda_{\Delta S}, \lambda_{s\phi}$ along with mixing angles. The signal strength of $h \rightarrow \gamma\gamma$ at LHC is given by

$$\mu_{\gamma\gamma} = \frac{\sigma_{\text{model}}(pp \rightarrow h \rightarrow \gamma\gamma)}{\sigma_{\text{SM}}(pp \rightarrow h \rightarrow \gamma\gamma)} \\ = \frac{\Gamma_{\text{model}}(h \rightarrow gg) \text{Br}(h \rightarrow \gamma\gamma)_{\text{model}}}{\Gamma_{\text{SM}}(h \rightarrow gg) \text{Br}(h \rightarrow \gamma\gamma)_{\text{SM}}} \\ = \cos \alpha_1^2 \cos \alpha_2^2 \frac{\text{Br}(h \rightarrow \gamma\gamma)_{\text{model}}}{\text{Br}(h \rightarrow \gamma\gamma)_{\text{SM}}}. \quad (37)$$

Similarly, we can write the signal strength of $h \rightarrow Z\gamma$ as

$$\mu_{Z\gamma} = \cos \alpha_1^2 \cos \alpha_2^2 \frac{\text{Br}(h \rightarrow Z\gamma)_{\text{model}}}{\text{Br}(h \rightarrow Z\gamma)_{\text{SM}}}. \quad (38)$$

The experimental bounds on the signal strengths are mentioned in Table I. In Fig. 1, the signal strength for $h \rightarrow \gamma\gamma$ is shown as a function of the triplet mass scale m_Δ . In the left panel, $\mu_{\gamma\gamma}$ is plotted as a function of m_Δ for different values of $\sin \alpha_2$. In the right panel, the signal strength of $h \rightarrow \gamma\gamma$ is plotted as a function of m_Δ for $\sin \alpha_2 = 0.01$ when different

mass gaps between the charged scalars are considered. Here, we see that as the dominant couplings that contribute to the decay widths heavily depend on the charged scalar masses, consideration of the nondegenerate mass of the triplet scalars provides us with an enlarged parameter space, which is consistent with the measurement of signal strength by ATLAS and CMS. Another important point to note is that consideration of the singlet scalar introduces an important parameter $\sin \alpha_2$ in the signal strength expression, which can affect the value of signal strength $\mu_{\gamma\gamma}$ as shown in the right panel of Fig. 1. Similar treatment for $\mu_{Z\gamma}$ is done in Fig. 2. Here, we see that while nondegeneracy of the charged scalars is considered, the model parameter space for m_Δ up to 600 GeV predicts a signal strength that is within 1σ deviation of the ATLAS measurement of signal strength and in 2σ limit of the CMS measurement of signal strength. Our model parameter space lies within 2σ limit of a recent combined analysis of ATLAS and CMS search data that show $\mu_{Z\gamma} = 2.2 \pm 0.7$ at the center of mass energy 13 TeV [54].

B. Theoretical constraints

- (i) *Vacuum stability conditions*: The stability of the potential demands that the quartic couplings and some of their combinations must be positive. These conditions ensure that the potential is bounded from below in any direction. The necessary copositivity conditions imposed on the model parameters are as follows:

TABLE I. Experimental signal strengths of $h \rightarrow \gamma\gamma$ and $h \rightarrow Z\gamma$ with uncertainties.

Signal strengths	$\mu_{\gamma\gamma}$	$\mu_{Z\gamma}$
ATLAS	$1.04^{+0.10}_{-0.09}$ [74]	$2.0^{+1.0}_{-0.9}$ [75]
CMS	$1.12^{+0.09}_{-0.09}$ [76]	$2.4^{+0.9}_{-0.9}$ [77]

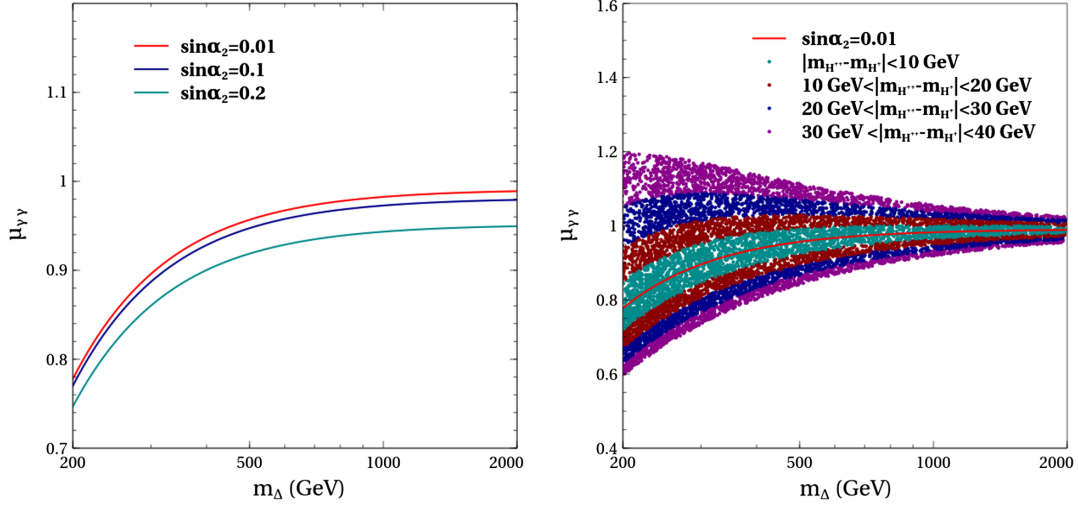


FIG. 1. $h \rightarrow \gamma\gamma$ signal strength as a function of triplet scale m_Δ . In the left panel, signal strength as a function of m_Δ ($= m_{H^{++}}, m_{H^\pm}, m_{H_1}, m_A$) for different values of $\sin\alpha_2$ mentioned inset. In the right panel, the same plot for $\sin\alpha_2 = 0.01$ with different values of the mass difference between charged scalars is considered. The other parameters are fixed at $\sin\alpha_1$ is 0.008, $\sin\alpha_3 = 0.001$, $v_s = 500$ GeV, $m_S = 200$ GeV taken for the plots.

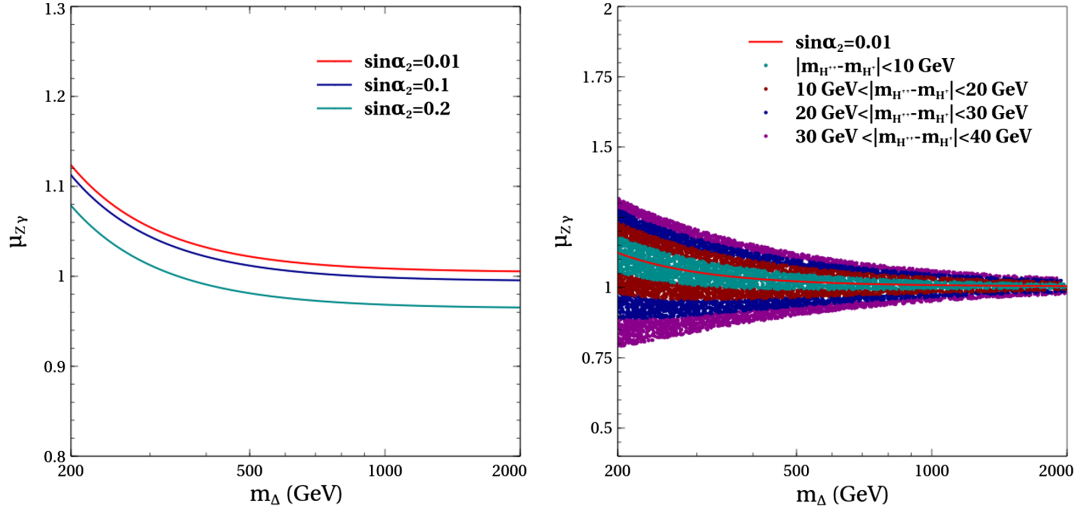


FIG. 2. $h \rightarrow Z\gamma$ signal strength as a function of triplet scale m_Δ . In the left panel, signal strength as a function of m_Δ ($= m_{H^{++}}, m_{H^\pm}, m_{H_1}, m_A$) for different values of $\sin\alpha_2$ mentioned inset. In the right panel, the same plot for $\sin\alpha_2 = 0.01$ with different values of the mass difference between charged scalars is considered. The value of $\sin\alpha_1$ is 0.008, $\sin\alpha_3 = 0.001$, $v_s = 500$ GeV, $m_S = 200$ GeV taken for the plots.

$$\lambda \geq 0, \quad \lambda_s \geq 0, \quad \lambda_2 + \lambda_3 \geq 0, \quad 2\lambda_2 + \lambda_3 \geq 0, \quad \lambda_{s\phi} + 2\sqrt{\lambda\lambda_s} \geq 0, \quad (39)$$

$$\lambda_{S\Delta} + 2\sqrt{(\lambda_2 + \lambda_3)\lambda_s} \geq 0, \quad \lambda_{S\Delta} + \sqrt{2(2\lambda_2 + \lambda_3)\lambda_s} \geq 0, \quad (40)$$

$$(\lambda_1 + \lambda_4) + 2\sqrt{(\lambda_2 + \lambda_3)\lambda} \geq 0, \quad \lambda_1 + 2\sqrt{\lambda(\lambda_2 + \lambda_3)} \geq 0, \quad (41)$$

$$(2\lambda_1 + \lambda_4) + 2\sqrt{2(2\lambda_2 + \lambda_3)\lambda} \geq 0, \quad \sqrt{2(\lambda_2 + \lambda_3)} + \sqrt{(\lambda_2 + \lambda_3)(2\lambda_2 + \lambda_3)} \geq 0. \quad (42)$$

(ii) *Perturbative unitarity*: It is also important to check whether the $2 \rightarrow 2$ scattering amplitudes involving the scalar fields satisfy unitarity constraints. Consequently, the parameters of the scalar potential are constrained from above as the following [78–80]:

$$\begin{aligned} \{|\lambda|, |\lambda_2|, |\lambda_s|, |(\lambda_2 + \lambda_3)|\} &\leq 4\pi, & \{|(2\lambda_1 - \lambda_4)|, |(2\lambda_1 + 3\lambda_4)|\} &\leq 16\pi, \\ \left\{|\lambda_1|, |(\lambda_1 + \lambda_4)|, |(2\lambda_2 - \lambda_3)|, |\lambda_{s\phi}|, |\lambda_{S\Delta}|, |(\lambda + \lambda_2 + 2\lambda_3) \pm \sqrt{(-\lambda + \lambda_2 + 2\lambda_3)^2 + \lambda_4^2}|\right\} &\leq 8\pi. \end{aligned} \quad (43)$$

The results noted in Eq. (43) have been obtained by a coupled channel analysis. However, some of the eigenvalues cannot be written in closed form. For such cases, we evaluate the eigenvalues of the coupled channel matrix numerically and impose the unitarity constraints. The form of the matrix is noted in Appendix A 3.

C. Effect of constraints on model parameter space

The experimental and theoretical conditions described in Sec. III put stringent constraints on the model parameter space. The aforementioned constraints on quartic couplings, in turn, can be translated on the physical parameters like masses and mixing, and in the following, we present such model parameter space.

The conditions on λ parameters prefer near mass degeneracy among the triplet dominated scalars. Figure 3 shows the allowed parameter space from unitarity and vacuum stability in the m_Δ vs $\sin\alpha_1$ plane. Here, we consider $\sin\alpha_2$ and $\sin\alpha_3$ to be zero, implying that S is completely decoupled from the triplet and the SM doublet. The magenta (cyan) colored points correspond to the case when $v_t = 2$ ($v_t = 1$) GeV. The choice of v_t has been made

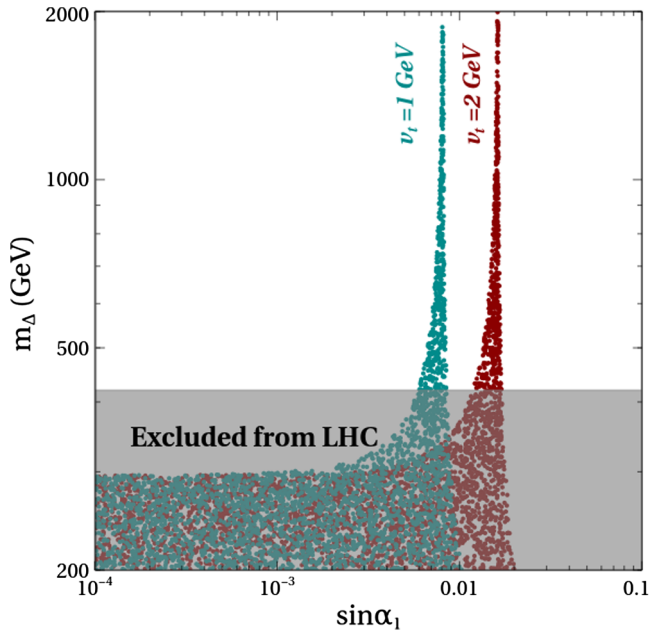


FIG. 3. Parameter space allowed from unitarity and vacuum stability conditions in m_Δ vs $\sin\alpha_1$ plane. The points with dark cyan color (dark red) correspond to $v_t = 1$ ($v_t = 2$) GeV. Here, $m_S = 200$ GeV and $v_s = 1000$ GeV, while the value of $\sin\alpha_2$ and $\sin\alpha_3$ are taken to be zero.

keeping it consistent with the ρ parameter constraint. We see in this plot that for a specific value of $\sin\alpha_1$ corresponding to each value of v_t , all values of m_Δ are allowed where $\sin\alpha_1 \sim (2v_t/v_d)$. For other values of $\sin\alpha_1$, $m_\Delta \leq 300$ GeV. This feature also has been observed in Ref. [81]. As $m_{H_1} \leq 300$ GeV is already excluded for the degenerate triplet dominated scalars from charged Higgs searches (see Sec. III A) (shown by the shaded region) and we are interested in the whole mass range of the triplet scalar for the analysis of DM phenomenology, we set $\sin\alpha_1$ as 0.008 for $v_t = 1$ GeV for the rest of this article.

In Fig. 4, we analyze the parametric dependence of $\sin\alpha_3$ and m_Δ on m_S vs $\sin\alpha_2$ plane coming from unitarity and vacuum stability constraints. In the left panel (right), m_Δ has been fixed at 450 GeV (750 GeV). The different colors in the figure correspond to different values of $\sin\alpha_3$. It is evident that with higher values of mixing angle $\sin\alpha_3$, the allowed masses of H_2 (m_S) become close to the mass scale of H_1 (m_Δ). As for example, in the left (right) panel, the allowed masses of m_S are close to 450 (750) GeV, which is the scale of the triplet mass when $\sin\alpha_3 = 0.01$.

In Fig. 5, we observe the effect of mixing angle $\sin\alpha_3$ in $|m_S - m_\Delta|$ vs m_S plane under the same theoretical constraints. Points with dark cyan color (dark red) correspond to $\sin\alpha_3 = 0.001$ ($\sin\alpha_3 = 0.01$). We see that the unitarity and vacuum stability constraints allow a mass difference $|m_S - m_\Delta| \lesssim 100$ GeV when $\sin\alpha_3 = 0.01$, whereas for $\sin\alpha_3 = 0.001$, the allowed mass difference is $|m_S - m_\Delta| \lesssim 1000$ GeV.

Now we will study the effect of v_s on our model parameter space. In Fig. 6, allowed parameter space from theoretical constraints is shown in m_S vs $\sin\alpha_2$ plane. The allowed region in m_S diminishes with smaller values of v_s for all possible values of mixing angle, $\sin\alpha_2$. λ_s , $\lambda_{s\phi}$, and $\lambda_{S\Delta}$ become smaller as v_s increases [see Eq. (A 1)]. Consequently, the unitarity constraints on such quartic parameters are automatically satisfied for higher values of v_s . This has been reflected in larger allowed regions in m_S vs $\sin\alpha_2$ plane for larger values of v_s . The shaded region shown in Figs. 4 and 6 comes from the exclusion limit of the mixing angle of a scalar singlet with SM Higgs from the LHC as mentioned in Sec. III A.

IV. DM PHENOMENOLOGY

Now we are equipped to discuss the DM phenomenology in this model. As a consequence of dark charge conjugation symmetry, Z' becomes stable and plays the role of DM in this framework. For a sizable value of new

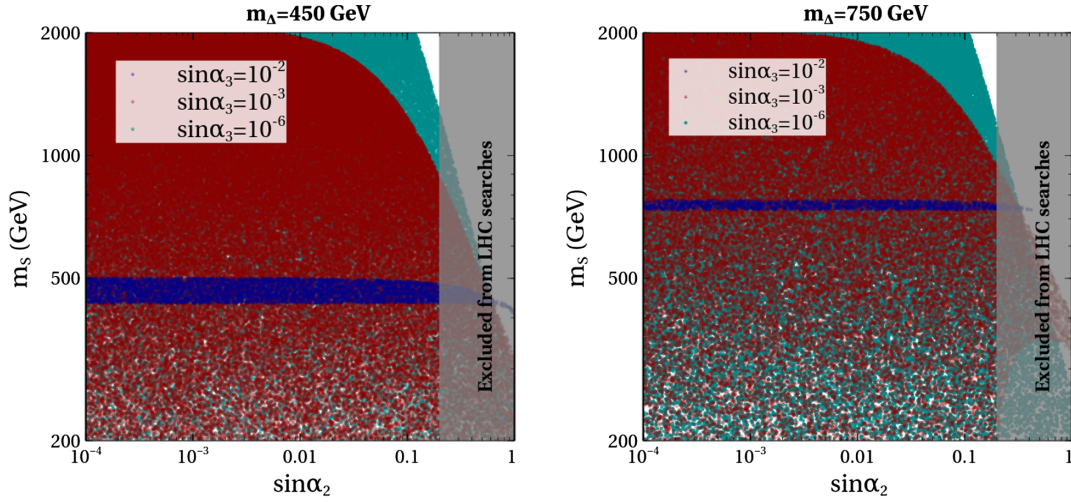


FIG. 4. Parameter space allowed from unitarity and vacuum stability conditions in m_S vs $\sin \alpha_2$ plane. The different colors correspond to different values of $\sin \alpha_3$ (mentioned inset). The value of v_s taken here is 1 TeV. For the left panel, $m_\Delta = 450$ GeV, whereas for the right panel, $m_\Delta = 750$ GeV. $\sin \alpha_1$ is set to be 0.008 corresponding to $v_t = 1$ GeV.

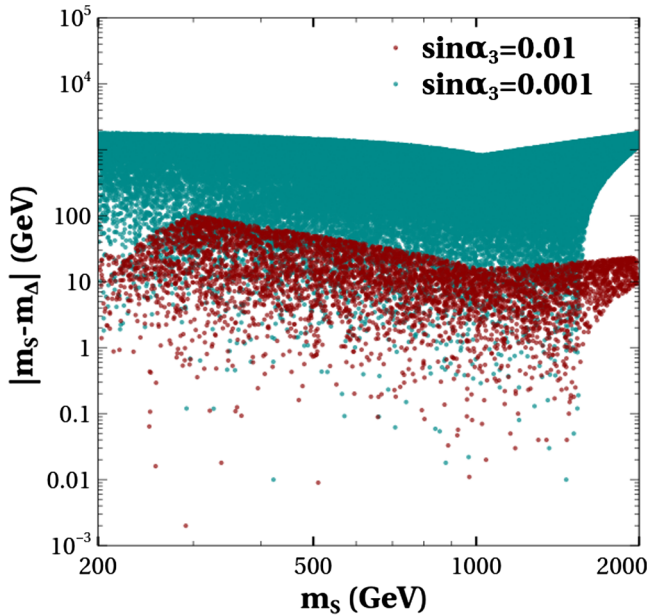


FIG. 5. Parameter space allowed from unitarity and vacuum stability conditions in $|m_S - m_\Delta|$ vs m_S plane. The points with dark cyan (dark red) color correspond to $\sin \alpha_3 = 0.001$ ($\sin \alpha_3 = 0.01$). The value of m_Δ taken here is 200 GeV and $v_s = 1000$ GeV, while the value of $\sin \alpha_1$ and $\sin \alpha_3$ are taken to be 0.008 and 0, respectively.

gauge coupling g_x , Z' can be present in the thermal bath of the early Universe via its interaction (mediated by S) with the SM fields. However, this is possible only when S itself is in thermal equilibrium with the SM fields. Thermalization of S is dominantly controlled by $\lambda_{s\phi}$. The annihilation channels that are responsible for keeping Z' and S in the thermal bath with the SM are shown in Fig. 7. We have chosen the model parameters in such a way that

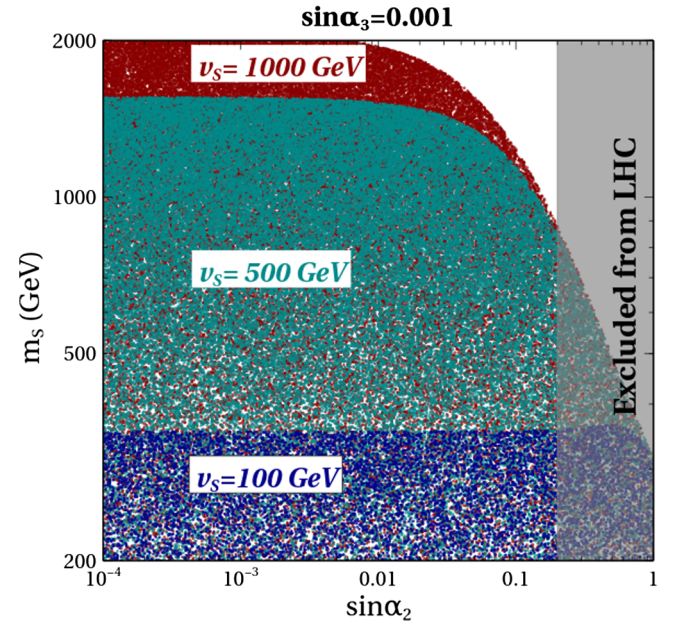


FIG. 6. Parameter space allowed from unitarity and vacuum stability conditions in m_S vs $\sin \alpha_2$ plane. The points with different colors correspond to different values of v_s . The value of m_Δ taken here is 430 GeV and $\sin \alpha_3 = 0.001$.

the $\lambda_{s\phi} \gtrsim 10^{-4}$ and g_x vary between (0–1). Such a choice of parameters ensures the thermalization of Z' in the early Universe. DM phenomenology is sensitive to the mass of DM (M'_Z), $U(1)_X$ gauge coupling (g_x), the mass of the singlet component dominated scalar (m_S), the mixing angles ($\sin \alpha_2, \sin \alpha_3$), and the mass of the triplet scalar (m_Δ).

The Boltzmann equation governing the comoving number density of Z' is given by

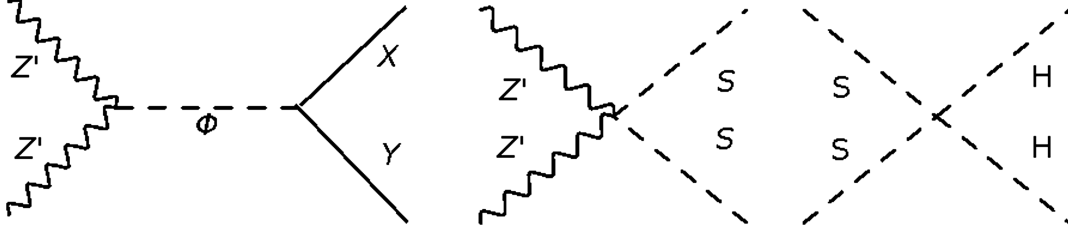


FIG. 7. Feynman diagrams that contribute to the thermalization of DM Z' . X and Y represent SM particles along with S (H_2) and triplet dominated scalars ($H_1, A_0, H^{\pm\pm}, H^{\pm}$). ϕ denotes h, H_1, H_2 .

$$\frac{dY_{Z'}}{dz} = -\langle\sigma_{Z'Z'\rightarrow XX}v_{\text{rel}}\rangle\frac{\beta s}{\mathcal{H}z}(Y_{Z'}^2 - Y_{Z'}^{\text{eq}2}), \quad (44)$$

where $Y_{Z'} = n_{Z'}/s$, the ratio of the number density of Z' and the entropy density of the visible sector and $z = m_S/T$. β is defined as $\beta = \frac{g_s^{1/2}(T)\sqrt{g_p(T)}}{g_s(T)}$, where g_s and g_p are degrees of freedom associated with entropy and energy densities, respectively, and $g_s^{1/2} = \frac{g_s}{\sqrt{g_p}}(1 + \frac{1}{3}\frac{T}{g_s}\frac{dg_s}{dT})$. The Hubble expansion rate \mathcal{H} is given by

$$\mathcal{H} = \sqrt{\frac{\pi^2 g_{\star\rho}}{90}} \frac{T^2}{M_{\text{Pl}}},$$

where $g_{\star\rho}$ is the total relativistic degrees of freedom at temperature T contributing to energy density, and $M_{\text{Pl}} = 2.4 \times 10^{18}$ GeV. $\langle\sigma_{Z'Z'\rightarrow XX}v_{\text{rel}}\rangle$ corresponds to the thermal average of annihilation cross section of Z' to SM fields and $H_1, A_0, H_2, H^{\pm\pm}, H^{\pm}$. The relic density $\Omega_{Z'}h^2$ and DD cross sections used in this analysis are calculated with the package micrOMEGAS (v5.3.41) [82] in

conjunction with FeynRules [83]. In the left panel of Fig. 8, we show how the relic abundance depends on $M_{Z'}$. The color bar represents the impact of g_x . m_Δ and m_S have been fixed at 400 GeV and 600 GeV, respectively. $\sigma_{Z'Z'\rightarrow SMSM}$ is greatly enhanced at $M_{Z'} = m_h/2, m_{H_1}/2$ and $m_{H_2}/2$, due to s -channel resonances (see Fig. 7). Consequently, relic density falls sharply at these values of $M_{Z'}$, as shown in Fig. 8. One can also note that relic density decreases with increasing g_x due to the enhanced annihilation rate of DM, which is the usual behaviour of WIMPs.

In the right panel of Fig. 8, we show the effect of mixing angles in the variation of relic density as a function of $M_{Z'}$. The masses of m_S and m_Δ are set at 400 GeV and 1000 GeV, respectively. The three colored lines in the figure correspond to three different choices of mixing angles $\sin\alpha_2$ and $\sin\alpha_3$. With the increment of the mixing angles $\sin\alpha_2$ and $\sin\alpha_3$, the S component increases in the physical scalars h and H_1 . Consequently, the rate of annihilation of DM via the mediation of these physical scalars increases, resulting in lower relic abundance of Z' . We see that for every line when $M_{Z'}$ crosses the mass of S , relic density falls due to the opening up of the dominant

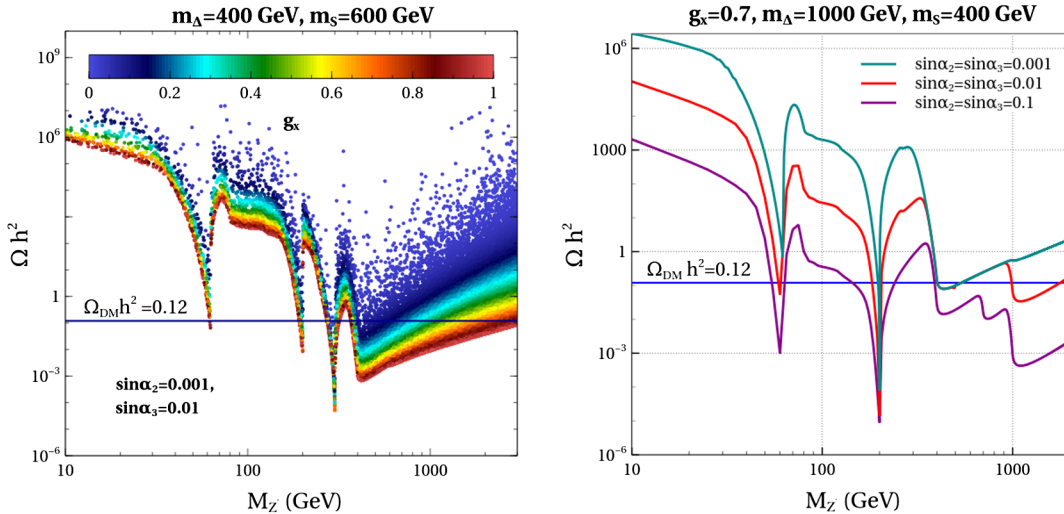


FIG. 8. Variation of relic abundance with the mass of DM. In the left panel, the value of m_Δ taken is 400 GeV and m_S is 600 GeV. The value of mixing angles are $\sin\alpha_2 = 0.001$ and $\sin\alpha_3 = 0.01$. The color bar corresponds to the variation of g_x . In the right panel, the value of m_Δ taken is 1000 GeV and m_S is 400 GeV. g_x is taken to be 0.7. The different colored line corresponds to different mixing angles which are mentioned inset.

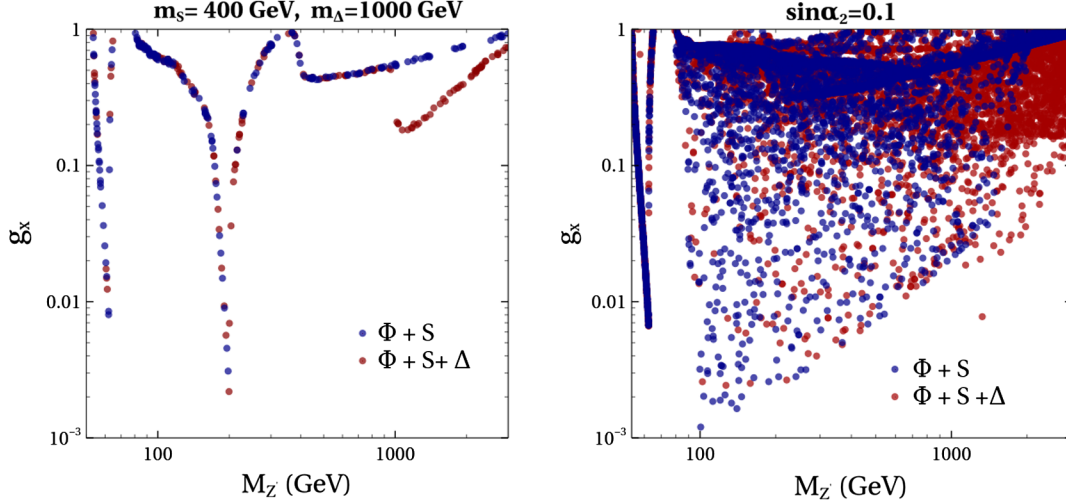


FIG. 9. Parameter space from relic density constraint in $M_{Z'}$ vs g_x plane. In the left panel, parameter space for correct relic abundance is shown for a fixed mass of m_S and m_Δ (mentioned inset). The dark blue points correspond to the conventional vector dark matter model, which has an extra SM singlet in the scalar sector, whereas the red points correspond to our scenario, which is extended by another $SU(2)_L$ scalar triplet in comparison to the former one. In the right panel, a similar plot has been shown when $m_S \in (200-3000)$ GeV and $m_\Delta \in (400-3000)$ GeV. $\sin \alpha_2 = 0.1$ is considered for both panels.

$Z'Z' \rightarrow H_2H_2$ annihilation channel. For $\sin \alpha_{2/3} = 0.001$, the effect of $Z'Z' \rightarrow H^{++}H^{--}/H^+H^-/H_1H_1$ channels are not observed, but for increasing mixing angles, the effect of these channels comes into play. The magenta line, which corresponds to mixing angles of 0.01, shows another low relic region just after $M_{Z'} > m_\Delta$, but the $\sin \alpha_{2/3} = 0.1$ line shows another interesting effect from the annihilation channel $Z'Z' \rightarrow H_1H_2$ when $2M_{Z'}$ becomes larger than the sum of masses of H_2 and H_1 ($m_\Delta + m_S$). Additional channels start to contribute to the annihilation of Z' significantly when we increase the mixing angles.

In Fig. 9, we show a comparison between the standard $U(1)_X$ extended vector dark matter model and our scenario from a dark matter perspective. The scalar sector of the former model consists of the SM Higgs doublet and a scalar singlet, whereas our scenario accommodates another $SU(2)_L$ triplet scalar along with the above-mentioned particles. In Fig. 9, in the left panel, allowed parameter space for correct relic abundance is shown for a fixed mass of m_S and m_Δ in $M_{Z'}$ vs g_x plane. The blue points correspond to the standard VDM with only an extra singlet scalar, whereas the red points correspond to our scenario (with an additional triplet). The first two resonance funnels in the plot appear due to SM Higgs and singlet scalar resonance, which are the same for the two scenarios. However, when $M_{Z'} > 700$ GeV, due to the opening of the extra channel $Z'Z' \rightarrow S\Delta$ in our scenario, relic density is satisfied for a lesser value of g_x . So, the allowed range of g_x for a particular value of $M_{Z'}$ increases. That result is also reflected in the right panel. The allowed parameter space from relic density constraint is shown by dark blue colored points (dark red points) for the minimal vector dark matter model (our scenario). We observe that the parameter space is larger

for our case, allowing lower values of g_x for higher DM mass ranges. This is due to the fact that adding an extra triplet Higgs in the scalar sector increases the parameter space by adding an extra resonance funnel region (see Fig. 8) along with providing new annihilation channels. $\sin \alpha_3 = 0.01$ and $\sin \alpha_2 = 0.1$ are considered for both the plots.

A. Detection aspects of DM

Dark matter detection can be classified broadly into three categories namely direct search, indirect search, and collider search. Direct search experiments measure the cross section of elastic scattering between DM and nucleons inside the detector material. Z' , in the present scenario, scatters off the nucleons via the mixing of S with SM Higgs. The Feynman diagram of the elastic scattering of DM to nucleons is shown in Fig. 10. The approximate expression of the cross section of this t -channel process is given by [23]

$$\sigma_{Z'N} \simeq \frac{\mu_{XN}^2}{\pi} \left(\frac{g_x \sin \alpha_2 \cos \alpha_2 m_p}{v_d} \right)^2 \left(\frac{1}{m_h^2} - \frac{1}{m_S^2} \right)^2 f_p^2, \quad (45)$$

where $\mu_{XN} = \frac{M_N M_{Z'}}{M_N + M_{Z'}}$ is reduced nucleon-DM mass, and $f_p = \sum_{q=u,d,s} f_q^p + 2/9(1 - \sum_{q=u,d,s} f_q^p) \simeq 0.468$ [84]. Here, the effect of H_1 has been neglected in the formula of the DD cross-section. H_1 , which is dominantly triplet, does have interaction with the nucleons or the DM suppressed by small factors involving mixing angles. As a result, the effective DM-nucleon scattering amplitude mediated by H_1 is proportional to $\sin \alpha_1 \sin \alpha_3$. Therefore, in the small $\sin \alpha$ limit, the effect of H_1 can be neglected in the DM nucleon scattering cross section.

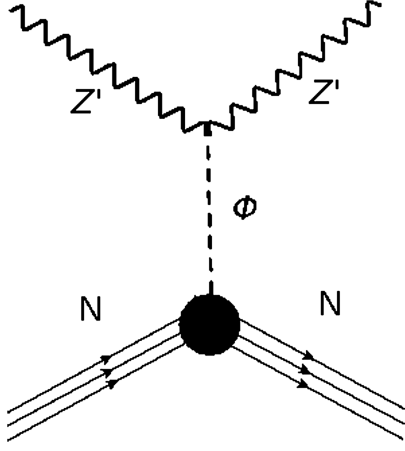


FIG. 10. Feynman diagram showing spin-independent elastic scattering of dark matter Z' with nucleons via CP even scalar ϕ where $\phi = h, H_1, H_2$.

As given in the Eq. (45), the direct search cross section is sensitive to the parameters $M_{Z'}$, g_x , $\sin \alpha_2$, and m_S . The product of g_x and $\sin \alpha_2$ act as the effective coupling here. By imposing the collider bound on $\sin \alpha_2$, we can have an upper bound on the maximum allowed value of g_x from DD limits. In Fig. 11, we show the bound on g_x for a particular $\sin \alpha_2$ over a model parameter space satisfying all other constraints mentioned. In the left panel of Fig. 11, we show the relic density satisfied parameter space in $M_{Z'}$ vs g_x plane for a range of scalar masses allowed by vacuum stability and unitarity for $\sin \alpha_2 = 0.1$. It is observed that the maximum allowed value of g_x is ~ 0.3 in this case from all constraints. The DD cross section from the LZ experiment gives the most stringent bound and XENON constraints next to it. The other bounds include Higgs invisible decay width, and the bound on v_s from unitarity though their effect becomes important for smaller $\sin \alpha_2$. In the

right panel of Fig. 11, we show the parameter space for $\sin \alpha_2 = 0.01$ in the same plane. Here, one can see that by lowering the value of $\sin \alpha_2$ by 1 order, the constraint on g_x is significantly relaxed from DD.

Indirect search provides a complementary way to look for DM in the Universe. WIMP annihilation in the galactic center, nearby galaxies, or the sun can produce observable fluxes of SM particles (photons, electrons, neutrinos, etc.), which can be detected at various telescopes, giving us information about DM distribution. Fermi-LAT, a satellite-based experimental facility, studies cosmic gamma-ray fluxes coming from the Galactic center. It provides the strongest bound on the rate of DM annihilation to photons for DM masses up to few hundreds of GeV [85]. In the present framework, the generation of monoenergetic and diffused photons from DM annihilation is driven by the processes $Z'Z' \rightarrow H_2 \rightarrow \gamma\gamma$ at one loop level and via $Z'Z' \rightarrow H_2 \rightarrow W^\pm W^\pm, H^\pm H^\mp, H^{\pm\pm} H^{\mp\mp}, f\bar{f}$ (with photons emitted from all external charged particles) if kinematically possible. However, the process $Z'Z' \rightarrow H_2 \rightarrow \gamma\gamma$ is not only loop suppressed but also subject to mixing angle suppression. The other channels are solely affected by mixing angle suppression. Consequently, due to the combined effects of loop and mixing angle suppression, both the line and diffuse gamma-ray fluxes resulting from dark matter annihilation in our model are significantly smaller than the limits indicated by Fermi-LAT data in the GeV mass ranges. Other important constraints as mentioned in [86] come from different experiments like CMB measurement by Planck, the Fermi detection of photons from the dwarf galaxies, the positron data from AMS-02, etc. However, in our model, as DM annihilates to nonstandard Higgses dominantly, so the direct production cross section of SM particles is well below the observed bounds.

Before we conclude this section, let us very briefly comment on the search prospect of the VDM at the LHC.

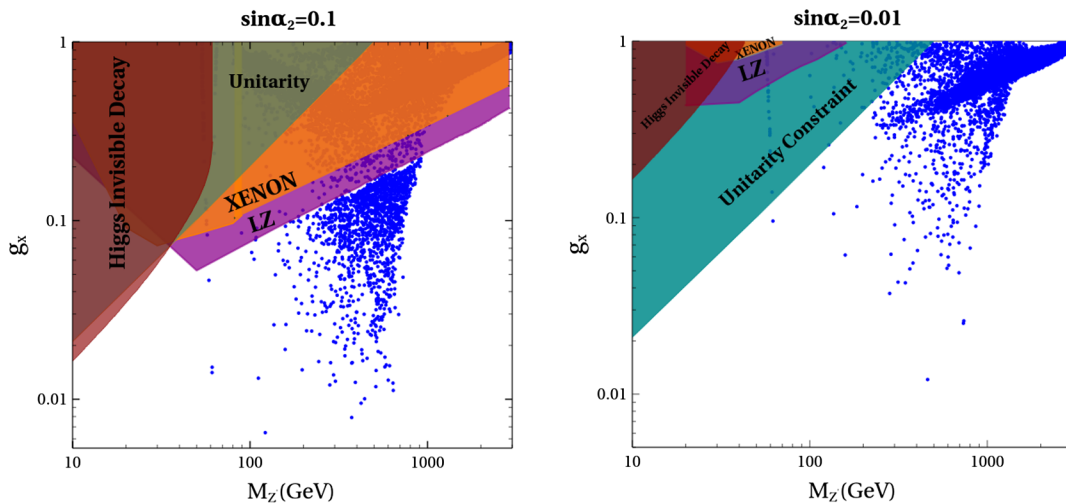


FIG. 11. Parameter space with all mentioned constraints in $M_{Z'}$ vs g_x plane for $\sin \alpha_2 = 0.1$ in the left panel. The colored region corresponds to exclusion from different constraints. In the right panel, the same plot for $\sin \alpha_2 = 0.01$.

Unfortunately, the direct production of a Z' pair in pp collision is prohibited by conservation of $U(1)_X$ charge. Z' pair can arise from the decay of H_2 , which can be produced in association with a Z boson at the LHC. In the allowed range of model parameters ($m_{H_2}, g_x, \sin \alpha_2$) from the constraints mentioned, the cross section is significantly small due to $\sin \alpha_2$ suppression. Another possible Z' signature can arise from the production of $H^{\pm\pm}$ in association with H^\mp followed by the decays of $H^{\pm\pm} \rightarrow W^\pm W^\pm$ and $H^\mp \rightarrow W^\mp H_2$ and further followed by $H_2 \rightarrow Z'Z'$. This final state would eventually result into *two dilepton + di-jet + missing energy* signature. This cross section is also very small due to the tiny $H^\mp \rightarrow W^\mp H_2$ suppressed branching ratio for allowed values of m_{H_2} at the LHC. It seems that the detection of our VDM at the LHC is very challenging unless a more innovative method is devised.

V. POSSIBILITY OF FREEZE-IN

In the previous section, we explored a scenario where the DM was initially in thermal equilibrium with the SM particle bath, but at a later time, it froze out as the interaction rate dropped below the expansion rate of the universe (\mathcal{H}). Due to such interaction with the SM particles, it can be probed by different DD experiments as we have shown earlier. However, the null results of all the DD experiments motivate us to explore another possibility where the interaction of DM with SM is so feeble that it never reaches the thermal equilibrium in the early universe. Rather, it could be produced from the decay or annihilation of the bath particles. Small value of coupling necessary for such feeble interaction can be naturally generated in a number of ways as shown in Ref. [87] in a flavor model context. Due to such feeble interactions, DM can evade the stringent DD constraints and

collider constraints. In this model, Z' can gain its number density in the early Universe from the decay of singlet scalar S (H_2) or annihilation of S (H_2). As S can be thermally produced through its interaction with SM Higgs, if the gauge coupling of $U(1)_X$, g_x is very small, typically in the order of $O(10^{-12})$, then Z' can never attain thermal equilibrium with the SM bath. With negligible initial abundance, DM gains its number density gradually from the decay of S . The decay of S is dictated by the vertex factor corresponding to $SZ'^\mu Z'_\mu \sim g_x^2 v_s$, whereas the annihilation of S is controlled by the vertex factor of $S^*SZ'^\mu Z'_\mu \sim g_x^2$. As the annihilation of S is suppressed by a v_s factor with respect to the decay at the vertex factor level, the decay term gives a dominant contribution to DM production. The mixing of S to other scalars being negligible S can be identified with mass eigenstate H_2 . To find out the DM number density evolution, we need to solve the Boltzmann equation for the number density of Z' . The Boltzmann equation in terms of DM comoving number density $Y_{Z'}$ is given by

$$\frac{dY_{Z'}}{dz} = \frac{\langle \Gamma_{S \rightarrow Z'Z'} \rangle}{\mathcal{H}z} Y_S^{\text{eq}}(z), \quad (46)$$

where z is $\frac{M_S}{T}$, $Y_{Z'}$ is the ratio of the comoving number density of DM to the entropy density of the visible sector, and Y_S^{eq} is the equilibrium co-moving number density of S , which is given by

$$Y_S^{\text{eq}} = \frac{45}{4\pi^4} \frac{g_s}{g_{*s}} (M_S/T)^2 K_2(M_S/T). \quad (47)$$

In the left panel of Fig. 12, we discuss the density evolution of our nonthermal DM candidate Z' by solving the Boltzmann equation. The solid lines correspond to the

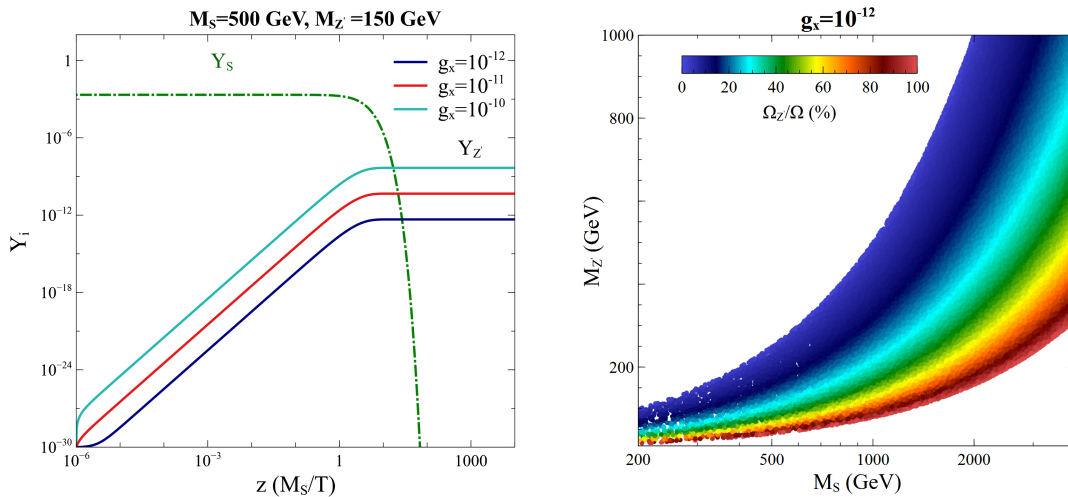


FIG. 12. Comoving number density evolution of DM and parent particle with $z = (M_S/T)$ in the left panel. The mass of Z' and S are mentioned inset. The solid lines correspond to DM number density $Y_{Z'}$ for different values of coupling g_x , whereas the dash-dotted line corresponds to the parent particle following the thermal bath. Allowed DM parameter space in M_S vs $M_{Z'}$ plane in the right panel. The color bar corresponds to the contribution of our DM candidate in total relic density in a percentage format.

DM number densities for different values of $U(1)_X$ coupling g_x . As the coupling g_x decreases, the decay width of S decreases; therefore, the final DM density achieved from the decay of S reduces. The dash-dotted line shows the number density of parent particle S , which follows thermal equilibrium. The DM abundance in this current era can be obtained as

$$\Omega_{Z'} h^2 = (2.755 \times 10^8) \frac{M_{Z'}}{\text{GeV}} Y_{Z'}^{\text{today}}, \quad (48)$$

Now comoving number density of DM Z' , $Y_{Z'}$ can be analytically expressed as [10]

$$Y_{Z'}^{\text{today}} \approx \frac{135 g_S}{8\pi^3 (1.66) g_{*s} \sqrt{g_*}} \frac{M_{PL}}{M_S^2} \Gamma_{S \rightarrow Z'Z'}, \quad (49)$$

which matches with our solution from the Boltzmann equation. In the right panel of Fig. 12, we show a region in M_S vs $M_{Z'}$ plane where Z' can contribute to the relic density through the decay of scalar S for $g_x = 10^{-12}$. The color bar corresponds to the percentage of relic density contribution of our DM candidate Z' . The region under the allowed parameter space is overabundant, whereas the upper region is excluded by kinematics ($2M_{Z'} \geq m_S$).

VI. CONCLUSION

To summarize, we have studied the phenomenology of a VDM in a gauged $U(1)_X$ extension of the SM set in a type II seesaw framework. The light neutrino masses are generated via the type-II seesaw mechanism by the introduction of an additional Higgs triplet (Δ). In the context of such a model, we investigate the possibility of a VDM, Z' , which is stabilized by an exact dark conjugation symmetry. Z' becomes massive when a complex scalar singlet S acquires VEV breaking the $U(1)_X$ symmetry spontaneously. We studied the possibility of both thermal and nonthermal production of Z' in the early Universe. Thermalization of Z' in the early Universe can be achieved for a sizable range of values of g_x (0–1) along with a comparatively smaller value of $\lambda_{s\phi}$ [$\mathcal{O}(10^{-4})$], the mixing between SM Higgs, and the additional singlet scalar (S). This mixing acts as a portal between the dark sector and the visible sector. To begin with, we have estimated the density of Z' in the present epoch by implementing our model in micromega. We have then shown a comparison between the relic density satisfied parameter space of our scenario and

that of the $U(1)_X$ extended minimal VDM model. We found out that our scenario allows lower g_x values for larger mass of DM due to the presence of newer annihilation channels with respect to the minimal model. The resulting relic density has been compared with available data reported by the PLANCK satellite. We have shown the implications of such a WIMP DM in light of the current limits of DD experiments like XENON and LZ. Due to the presence of the triplet scalar, necessary for neutrino mass generation, the vacuum stability and unitarity constraints on λ parameters are restrictive. Our model parameter space satisfies constraints from vacuum stability, perturbative unitarity, ρ parameter, oblique parameters, lepton flavor violation from charged scalars, and Higgs invisible decay. This framework can also accommodate the existing 2σ deviation observed in the $h \rightarrow Z\gamma$ decay rate over a wide range of parameter space. We have shown that after considering all the aforementioned constraints, the upper limit of g_x is nearly 0.3 for DM masses in the range (100–1000) GeV when $\sin \alpha_2 = 0.1$. However, such an upper limit on g_x crucially depends on $\sin \alpha_2$ and becomes weaker for lower values of $\sin \alpha_2$ as evident from Fig. 11. In the end, we briefly discussed the possibility of nonthermal production of Z' from the decay of the complex scalar S . For the values of g_x as small as 10^{-12} , the allowed mass range of DM varies between (100–300) GeV when Z' contributes 100% to the relic density.

ACKNOWLEDGMENTS

The authors would like to thank Dilip Kumar Ghosh for various useful discussions during this work. N. D. would like to thank Pooja Bhattacharjee for useful discussions. N. D. is funded by CSIR, Government of India, under the NET SRF fellowship scheme with Award file No. 09/080(1187)/2021-EMR-I. T. J. acknowledges the support from the Science and Engineering Research Board (SERB), Government of India under Grant Reference No. PDF/2020/001053. The work of D. N. is supported by the National Research Foundation of Korea (NRF) Research Grant No. NRF-2019R1A2C3005009 (DN).

APPENDIX

1. Expression for λ parameters

The λ parameters in terms of masses of physical scalars and mixing angles can be expressed as

$$\lambda = \frac{1}{2v_d^2} \{ m_h^2 c_{\alpha_1}^2 c_{\alpha_2}^2 + s_{\alpha_1}^2 (m_{H_1}^2 c_{\alpha_3}^2 + m_{H_2}^2 s_{\alpha_3}^2) + c_{\alpha_1}^2 s_{\alpha_2}^2 (m_{H_1}^2 s_{\alpha_3}^2 + m_{H_2}^2 c_{\alpha_3}^2) - (m_{H_2}^2 - m_{H_1}^2) c_{\alpha_1} s_{\alpha_1} s_{\alpha_2} s_{2\alpha_3} \}, \quad (A1)$$

$$\lambda_1 = \frac{1}{v_d v_t} \{ m_h^2 c_{\alpha_1} s_{\alpha_1} c_{\alpha_2}^2 - m_{H_1}^2 (s_{\alpha_1} c_{\alpha_3} + c_{\alpha_1} s_{\alpha_2} s_{\alpha_3}) (c_{\alpha_1} c_{\alpha_3} - s_{\alpha_1} s_{\alpha_2} s_{\alpha_3}) + m_{H_2}^2 (s_{\alpha_1} s_{\alpha_2} c_{\alpha_3} + c_{\alpha_1} s_{\alpha_3}) (c_{\alpha_1} s_{\alpha_2} c_{\alpha_3} - s_{\alpha_1} s_{\alpha_3}) \} + 2 \left\{ \frac{2m_{H^\pm}^2}{v_d^2 + 2v_t^2} - \frac{m_A^2}{v_d^2 + 4v_t^2} \right\}, \quad (\text{A2})$$

$$\lambda_2 = \frac{1}{2v_t^2} \{ m_h^2 s_{\alpha_1}^2 c_{\alpha_2}^2 + m_{H_1}^2 (c_{\alpha_1} c_{\alpha_3} - s_{\alpha_1} s_{\alpha_2} s_{\alpha_3})^2 + m_{H_2}^2 (c_{\alpha_1} s_{\alpha_3} + s_{\alpha_1} s_{\alpha_2} c_{\alpha_3})^2 \} + \frac{v_d^2}{2v_t^2} \left\{ \frac{m_A^2}{v_d^2 + 4v_t^2} - \frac{4m_{H^\pm}^2}{v_d^2 + 2v_t^2} \right\} + \frac{m_{H^{\pm\pm}}^2}{v_t^2}, \quad (\text{A3})$$

$$\lambda_3 = \frac{1}{v_t^2} \left\{ \frac{2v_d^2 m_{H^\pm}^2}{v_d^2 + 2v_t^2} - m_{H^{\pm\pm}}^2 - \frac{v_d^2 m_A^2}{v_d^2 + 4v_t^2} \right\} \quad (\text{A4})$$

$$\lambda_4 = \frac{4m_A^2}{v_d^2 + 4v_t^2} - \frac{4m_{H^\pm}^2}{v_d^2 + 2v_t^2} \quad (\text{A5})$$

$$\mu = \frac{\sqrt{2} m_{A^0} v_t}{v_d^2 + 4v_t^2} \quad (\text{A6})$$

$$\lambda_s = \frac{1}{2v_s^2} \{ m_h^2 s_{\alpha_2}^2 + c_{\alpha_2}^2 (m_{H_1}^2 s_{\alpha_3}^2 + m_{H_2}^2 c_{\alpha_3}^2) \},$$

$$\lambda_{s\phi} = \frac{c_{\alpha_2}}{v_d v_s} \{ (m_{H_2}^2 - m_{H_1}^2) s_{\alpha_1} s_{\alpha_3} c_{\alpha_3} + c_{\alpha_1} s_{\alpha_2} (m_h^2 - m_{H_1}^2 s_{\alpha_3}^2 - m_{H_2}^2 c_{\alpha_3}^2) \}, \quad (\text{A7})$$

$$\lambda_{S\Delta} = \frac{c_{\alpha_2}}{v_t v_s} \{ (m_{H_1}^2 - m_{H_2}^2) c_{\alpha_1} s_{\alpha_3} c_{\alpha_3} + s_{\alpha_1} s_{\alpha_2} (m_h^2 - m_{H_1}^2 s_{\alpha_3}^2 - m_{H_2}^2 c_{\alpha_3}^2) \}. \quad (\text{A8})$$

2. $h \rightarrow \gamma\gamma$ and $h \rightarrow Z\gamma$ accessories

The loop functions for the spin-0, spin-1/2 and spin-1 particles are given by

$$A_0^h(\tau) = -[\tau - f(\tau)]\tau^{-2}, \quad (\text{A9})$$

$$A_{1/2}^h(\tau) = 2[\tau + (\tau - 1)f(\tau)]\tau^{-2}, \quad (\text{A10})$$

$$A_1^h(\tau) = -[2\tau^2 + 3\tau + 3(2\tau - 1)f(\tau)]\tau^{-2}, \quad (\text{A11})$$

where

$$f(\tau) = \begin{cases} [\sin^{-1}(\sqrt{\tau})]^2 & (\tau \leq 1) \\ -\frac{1}{4} \left[\log \left(\frac{1 + \sqrt{1 - \tau^{-1}}}{1 - \sqrt{1 - \tau^{-1}}} \right) - i\pi \right]^2 & (\tau > 1). \end{cases}$$

$g_{hf\bar{f}}$ and $g_{hW^+W^-}$ correspond to the relative coupling of mass eigenstate h to the SM Higgs coupling. The relative couplings in terms of our set of free parameters can be written as

$$g_{hf\bar{f}} = \frac{\cos \alpha_1 \cos \alpha_2}{\cos \beta'},$$

$$g_{hW^+W^-} = \frac{2v_t \sin \alpha_1 \cos \alpha_2}{v_d} + \cos \alpha_1 \cos \alpha_2. \quad (\text{A12})$$

Here, we can see that when $\sin \alpha_2$ tends to zero, we get back our pure type II seesaw couplings (see Ref. [58]). In the limit, $\sin \alpha_1 \rightarrow 0$, $\sin \alpha_2 \rightarrow 0$ and $v_t \ll v_d$, $\cos \beta' \rightarrow 0$ and the relative couplings become one; hence, the SM Higgs coupling are restored. The scalar trilinear couplings $\tilde{g}_{hH^\pm H^\mp}$ and $\tilde{g}_{hH^{\pm\pm}H^{\mp\mp}}$ are given by

$$\tilde{g}_{hH^{++}H^{--}} = \frac{m_w}{gm_{H^{\pm\pm}}^2} g_{hH^{++}H^{--}}, \quad \tilde{g}_{hH^+H^-} = \frac{m_w}{gm_{H^\pm}^2} g_{hH^+H^-}, \quad (\text{A13})$$

with $g_{hH^{++}H^{--}}$ and $g_{hH^+H^-}$ given by

$$\begin{aligned}
g_{hH^{++}H^{--}} &= \lambda_1 v_d \cos \alpha_1 \cos \alpha_2 + 2\lambda_2 v_t \sin \alpha_1 \cos \alpha_2 + \lambda_{\Delta S} v_s \sin \alpha_2 \\
g_{hH^+H^-} &= \frac{1}{2} \left\{ 4(\lambda_2 + \lambda_3) v_t \cos^2 \beta' \cos \alpha_2 + 2\lambda_1 v_t \sin^2 \beta' \sin \alpha_1 \cos \alpha_2 + \frac{1}{\sqrt{2}} \lambda_4 v_d \sin 2\beta' \sin \alpha_1 \cos \alpha_2 \right. \\
&\quad + \cos \alpha_1 \cos \alpha_2 (4\lambda v_d \sin^2 \beta' + (2\lambda_1 + \lambda_4) v_d \cos^2 \beta' + (4\mu - \sqrt{2}\lambda_4 v_t) \cos \beta' \sin \beta') \\
&\quad \left. + 2 \sin \alpha_2 (\lambda_{\Delta S} \cos^2 \beta' + \lambda_{s\phi} \sin^2 \beta') \right\}. \tag{A14}
\end{aligned}$$

The terms including $\lambda_{\Delta S}$ and $\lambda_{s\phi}$ come from the extra complex singlet scalar sector, and a factor of $\cos \alpha_2$ appears with the rest of the part due to its mixing with the SM doublet. In the limit $\sin \alpha_2 \rightarrow 0$, these couplings reduce to doublet triplet Higgs model couplings as mentioned in [88]. The necessary loop functions and couplings for $h \rightarrow Z\gamma$ are mentioned below. The loop factors for particles with different spins are given by

$$\begin{aligned}
A_0^h(\tau_h, \tau_Z) &= I_1(\tau_h, \tau_Z) \\
A_{1/2}^h(\tau_h, \tau_Z) &= I_1(\tau_h, \tau_Z) - I_2(\tau_h, \tau_Z) \\
A_1^h(\tau_h, \tau_Z) &= 4(3 - \tan^2 \theta_W) I_2(\tau_h, \tau_Z) + [(1 + 2\tau_h^{-1}) \tan^2 \theta_W - (5 + 2\tau_h^{-1})] I_1(\tau_h, \tau_Z), \tag{A15}
\end{aligned}$$

where the I_1 and I_2 are given by

$$\begin{aligned}
I_1(\tau_h, \tau_Z) &= \frac{\tau_h \tau_Z}{2(\tau_h - \tau_Z)} + \frac{\tau_h^2 \tau_Z^2}{2(\tau_h - \tau_Z)^2} [f[\tau_h^{-1}] - f[\tau_Z^{-1}]] + \frac{\tau_h^2 \tau_Z}{(\tau_h - \tau_Z)^2} [g(\tau_h^{-1}) - g(\tau_Z^{-1})], \\
I_2(\tau_h, \tau_Z) &= -\frac{\tau_h \tau_Z}{2(\tau_h - \tau_Z)} [f[\tau_h^{-1}] - f[\tau_Z^{-1}]]. \tag{A16}
\end{aligned}$$

Here, the function $g(\tau)$ is given by

$$g(\tau) = \begin{cases} \sqrt{\tau^{-1} - 1} \sin^{-1}(\sqrt{\tau}) & (\tau < 1) \\ \frac{1}{2} \sqrt{1 - \tau^{-1}} \left[\log \left(\frac{1 + \sqrt{1 - \tau^{-1}}}{1 - \sqrt{1 - \tau^{-1}}} \right) - i\pi \right]^2 & (\tau \geq 1). \end{cases}$$

The function $f(\tau)$, couplings $g_{hf\bar{f}}$ and $g_{hW^+W^-}$ are given in Eq. (A12). The coupling $g_{ZH^+H^-}$ and $g_{ZH^{++}H^{--}}$ are given by

$$g_{ZH^+H^-} = -\tan \theta_W, \quad g_{ZH^{++}H^{--}} = 2 \cot 2\theta_W. \tag{A17}$$

3. Unitarity constraints

The unitary bounds of the model are extracted from the amplitude matrix ($2 \rightarrow 2$ scattering amplitude) where the basis eigenvector is made of all possible two particle states. Each eigenvalue of this matrix should be less than 8π to satisfy unitarity. The amplitude matrix can be decomposed into nine charge neutral, 14 singly charged, and nine doubly charged two particle states. We have calculated the conditions following the prescription of Ref. [89], which have been mentioned in the main text. However, the amplitude matrix corresponding to the charge neutral scatterings does not give the closed form of eigenvalues and therefore we solve the matrix numerically. The charge neutral two particle states with identical particles are given by

$$|\Delta^{++}\Delta^{--}\rangle, \quad |\Delta^+\Delta^-\rangle, \quad |\phi^+\phi^-\rangle, \quad |g_0g_0\rangle, \quad |\eta_0\eta_0\rangle, \quad |h_0h_0\rangle, \quad |\delta_0\delta_0\rangle, \quad |s_r s_r\rangle, |s_i s_i\rangle.$$

The amplitude matrix in the above basis is given by

$$M = \begin{pmatrix} 4(\lambda_2 + \lambda_3) & 2(\lambda_2 + \lambda_3) & \lambda_1 + \lambda_4 & \frac{\lambda_1}{\sqrt{2}} & \frac{\lambda_1}{\sqrt{2}} & \sqrt{2}\lambda_2 & \sqrt{2}\lambda_2 & \frac{\lambda_{\Delta_s}}{\sqrt{2}} & \frac{\lambda_{\Delta_s}}{\sqrt{2}} \\ 2(\lambda_2 + \lambda_3) & 4\lambda_2 + \frac{\lambda_3}{2} & \lambda_1 + \frac{\lambda_4}{2} & \frac{2\lambda_1 + \lambda_4}{2\sqrt{2}} & \frac{2\lambda_1 + \lambda_4}{2\sqrt{2}} & \sqrt{2}(\lambda_2 + \lambda_3) & \sqrt{2}(\lambda_2 + \lambda_3) & \frac{\lambda_{\Delta_s}}{\sqrt{2}} & \frac{\lambda_{\Delta_s}}{\sqrt{2}} \\ \lambda_1 + \lambda_4 & \lambda_1 + \frac{\lambda_4}{2} & 4\lambda & \sqrt{2}\lambda & \sqrt{2}\lambda & \frac{\lambda_1}{\sqrt{2}} & \frac{\lambda_1}{\sqrt{2}} & \frac{\lambda_{\Phi_s}}{\sqrt{2}} & \frac{\lambda_{\Phi_s}}{\sqrt{2}} \\ \frac{\lambda_1}{\sqrt{2}} & \frac{2\lambda_1 + \lambda_4}{2\sqrt{2}} & \sqrt{2}\lambda & 3\lambda & \lambda & \frac{\lambda_1 + \lambda_4}{2} & \frac{\lambda_1 + \lambda_4}{2} & \frac{\lambda_{\Phi_s}}{\sqrt{2}} & \frac{\lambda_{\Phi_s}}{\sqrt{2}} \\ \frac{\lambda_1}{\sqrt{2}} & \frac{2\lambda_1 + \lambda_4}{2\sqrt{2}} & \sqrt{2}\lambda & \lambda & 3\lambda & \frac{\lambda_1 + \lambda_4}{2} & \frac{\lambda_1 + \lambda_4}{2} & \frac{\lambda_{\Phi_s}}{\sqrt{2}} & \frac{\lambda_{\Phi_s}}{\sqrt{2}} \\ \sqrt{2}\lambda_2 & \sqrt{2}(\lambda_2 + \lambda_3) & \frac{\lambda_1}{\sqrt{2}} & \frac{\lambda_1 + \lambda_4}{2} & \frac{\lambda_1 + \lambda_4}{2} & 3(\lambda_2 + \lambda_3) & \lambda_2 + \lambda_3 & \frac{\lambda_{\Delta_s}}{2} & \frac{\lambda_{\Delta_s}}{2} \\ \sqrt{2}\lambda_2 & \sqrt{2}(\lambda_2 + \lambda_3) & \frac{\lambda_1}{\sqrt{2}} & \frac{\lambda_1 + \lambda_4}{2} & \frac{\lambda_1 + \lambda_4}{2} & \lambda_2 + \lambda_3 & 3(\lambda_2 + \lambda_3) & \frac{\lambda_{\Delta_s}}{2} & \frac{\lambda_{\Delta_s}}{2} \\ \frac{\lambda_{\Delta_s}}{\sqrt{2}} & \frac{\lambda_{\Delta_s}}{\sqrt{2}} & \frac{\lambda_{\Phi_s}}{\sqrt{2}} & \frac{\lambda_{\Phi_s}}{2} & \frac{\lambda_{\Phi_s}}{2} & \frac{\lambda_{\Delta_s}}{2} & \frac{\lambda_{\Delta_s}}{2} & 3\lambda_s & \lambda_s \\ \frac{\lambda_{\Delta_s}}{\sqrt{2}} & \frac{\lambda_{\Delta_s}}{\sqrt{2}} & \frac{\lambda_{\Phi_s}}{\sqrt{2}} & \frac{\lambda_{\Phi_s}}{2} & \frac{\lambda_{\Phi_s}}{2} & \frac{\lambda_{\Delta_s}}{2} & \frac{\lambda_{\Delta_s}}{2} & \lambda_s & 3\lambda_s \end{pmatrix}. \quad (\text{A18})$$

4. Decay widths

The partial decay width of SM Higgs h and singlet scalar H_2 to the gauge boson Z' is given by

$$\Gamma(h \rightarrow Z'Z') = \frac{g_x^2 \sin^2 \alpha_2 M_{Z'}^2}{8\pi m_h} \sqrt{1 - \frac{4M_{Z'}^2}{m_h^2}} \left(2 + \frac{m_h^4}{4M_{Z'}^4} \left(1 - \frac{2M_{Z'}^2}{m_h^2} \right)^2 \right), \quad (\text{A19})$$

$$\Gamma(H_1 \rightarrow Z'Z') = \frac{g_x^2 \cos^2 \alpha_2 \sin^2 \alpha_3 M_{Z'}^2}{8\pi m_{H_1}} \sqrt{1 - \frac{4M_{Z'}^2}{m_{H_1}^2}} \left(2 + \frac{m_{H_1}^4}{4M_{Z'}^4} \left(1 - \frac{2M_{Z'}^2}{m_{H_1}^2} \right)^2 \right), \quad (\text{A20})$$

$$\Gamma(H_2 \rightarrow Z'Z') = \frac{g_x^2 \cos^2 \alpha_2 \cos^2 \alpha_3 M_{Z'}^2}{8\pi m_{H_2}} \sqrt{1 - \frac{4M_{Z'}^2}{m_{H_2}^2}} \left(2 + \frac{m_{H_2}^4}{4M_{Z'}^4} \left(1 - \frac{2M_{Z'}^2}{m_{H_2}^2} \right)^2 \right). \quad (\text{A21})$$

5. Interaction rates

The thermally averaged decay width of S is given by

$$\langle \Gamma_{S \rightarrow Z'Z'} \rangle = \frac{K_1(M_S/T)}{K_2(M_S/T)} \Gamma_{S \rightarrow Z'Z'}. \quad (\text{A22})$$

-
- [1] F. Zwicky, *Helv. Phys. Acta* **6**, 110 (1933).
 [2] V. C. Rubin and W. K. Ford, Jr., *Astrophys. J.* **159**, 379 (1970).
 [3] D. Clowe, M. Bradac, A. H. Gonzalez, M. Markevitch, S. W. Randall, C. Jones, and D. Zaritsky, *Astrophys. J. Lett.* **648**, L109 (2006).
 [4] D. N. Spergel *et al.* (WMAP Collaboration), *Astrophys. J. Suppl. Ser.* **170**, 377 (2007).
 [5] L. Roszkowski, E. M. Sessolo, and S. Trojanowski, *Rep. Prog. Phys.* **81**, 066201 (2018).
 [6] N. Aghanim *et al.* (Planck Collaboration), *Astron. Astrophys.* **641**, A6 (2020); **652**, C4(E) (2021).
 [7] G. Bertone, D. Hooper, and J. Silk, *Phys. Rep.* **405**, 279 (2005).
 [8] W. Hu and S. Dodelson, *Annu. Rev. Astron. Astrophys.* **40**, 171 (2002).

- [9] E. W. Kolb and M. S. Turner, *The Early Universe* (1990), Vol. 69, ISBN 978-0-201-62674-2.
- [10] L. J. Hall, K. Jedamzik, J. March-Russell, and S. M. West, *J. High Energy Phys.* **03** (2010) 080.
- [11] Y. Hochberg, E. Kuflik, T. Volansky, and J. G. Wacker, *Phys. Rev. Lett.* **113**, 171301 (2014).
- [12] S. Dimopoulos, D. Eichler, R. Esmailzadeh, and G. D. Starkman, *Phys. Rev. D* **41**, 2388 (1990).
- [13] J. L. Feng, A. Rajaraman, and F. Takayama, *Phys. Rev. Lett.* **91**, 011302 (2003).
- [14] M. Pospelov, A. Ritz, and M. B. Voloshin, *Phys. Rev. D* **78**, 115012 (2008).
- [15] M. Pospelov, A. Ritz, and M. B. Voloshin, *Phys. Lett. B* **662**, 53 (2008).
- [16] R. T. D’Agnolo, D. Liu, J. T. Ruderman, and P.-J. Wang, *J. High Energy Phys.* **06** (2021) 103.
- [17] D. S. Akerib *et al.* (LUX Collaboration), *Phys. Rev. Lett.* **118**, 021303 (2017).
- [18] E. Aprile *et al.* (XENON Collaboration), *Phys. Rev. Lett.* **121**, 111302 (2018).
- [19] E. Aprile *et al.* (XENON Collaboration), *Phys. Rev. Lett.* **131**, 041003 (2023).
- [20] A. Tan *et al.* (PandaX-II Collaboration), *Phys. Rev. Lett.* **117**, 121303 (2016).
- [21] X. Cui *et al.* (PandaX-II Collaboration), *Phys. Rev. Lett.* **119**, 181302 (2017).
- [22] J. Aalbers *et al.* (LZ Collaboration), *Phys. Rev. Lett.* **131**, 041002 (2023).
- [23] S. Baek, P. Ko, W.-I. Park, and E. Senaha, *J. High Energy Phys.* **05** (2013) 036.
- [24] Y. Farzan and A. R. Akbarieh, *J. Cosmol. Astropart. Phys.* **10** (2012) 026.
- [25] N. Baouche, A. Ahriche, G. Faisel, and S. Nasri, *Phys. Rev. D* **104**, 075022 (2021).
- [26] T. Nomura, H. Okada, and S. Yun, *J. High Energy Phys.* **06** (2021) 122.
- [27] K. S. Babu, S. Jana, and A. Thapa, *J. High Energy Phys.* **02** (2022) 051.
- [28] B. Barman, S. Bhattacharya, S. K. Patra, and J. Chakraborty, *J. Cosmol. Astropart. Phys.* **12** (2017) 021.
- [29] M. Duch, B. Grzadkowski, and M. McGarrie, *J. High Energy Phys.* **09** (2015) 162.
- [30] A. Amiri, B. Díaz Sáez, and K. Ghorbani, *Phys. Lett. B* **844**, 138119 (2023).
- [31] P. D. Group, P. A. Zyla, R. M. Barnett, J. Beringer, O. Dahl, D. A. Dwyer, D. E. Groom, C. J. Lin, K. S. Lugovsky, E. Pianori *et al.*, *Prog. Theor. Exp. Phys.* **2020**, 083C01 (2020).
- [32] R. N. Mohapatra *et al.*, *Rep. Prog. Phys.* **70**, 1757 (2007).
- [33] P. Minkowski, *Phys. Lett. B* **67**, 421 (1977).
- [34] T. Yanagida, *Conf. Proc. C* **7902131**, 95 (1979).
- [35] M. Gell-Mann, P. Ramond, and R. Slansky, *Conf. Proc. C* **790927**, 315 (1979).
- [36] R. N. Mohapatra and G. Senjanovic, *Phys. Rev. Lett.* **44**, 912 (1980).
- [37] M. Magg and C. Wetterich, *Phys. Lett. B* **94**, 61 (1980).
- [38] G. Lazarides, Q. Shafi, and C. Wetterich, *Nucl. Phys.* **B181**, 287 (1981).
- [39] R. N. Mohapatra and G. Senjanović, *Phys. Rev. D* **23**, 165 (1981).
- [40] J. Schechter and J. W. F. Valle, *Phys. Rev. D* **22**, 2227 (1980).
- [41] T. P. Cheng and L.-F. Li, *Phys. Rev. D* **22**, 2860 (1980).
- [42] R. N. Mohapatra and G. Senjanović, *Phys. Rev. Lett.* **44**, 912 (1980).
- [43] E. Ma, *Phys. Rev. Lett.* **81**, 1171 (1998).
- [44] R. Foot, H. Lew, X. G. He, and G. C. Joshi, *Z. Phys. C* **44**, 441 (1989).
- [45] E. Ma and U. Sarkar, *Phys. Rev. Lett.* **80**, 5716 (1998).
- [46] E. Ma and D. P. Roy, *Nucl. Phys.* **B644**, 290 (2002).
- [47] T. Hambye, Y. Lin, A. Notari, M. Papucci, and A. Strumia, *Nucl. Phys.* **B695**, 169 (2004).
- [48] N. Okada, S. Okada, and D. Raut, *Phys. Rev. D* **100**, 035022 (2019).
- [49] N. Okada and O. Seto, *Phys. Rev. D* **101**, 023522 (2020).
- [50] N. Okada, S. Okada, D. Raut, and Q. Shafi, *Phys. Lett. B* **810**, 135785 (2020).
- [51] S. Ashanujjaman and K. Ghosh, *J. High Energy Phys.* **03** (2022) 195.
- [52] N. Okada and O. Seto, *Phys. Rev. D* **105**, 123512 (2022).
- [53] P. Ghosh, S. Mahapatra, N. Narendra, and N. Sahu, *Phys. Rev. D* **106**, 015001 (2022).
- [54] G. Aad *et al.* (ATLAS, CMS Collaborations), *Phys. Rev. Lett.* **132**, 021803 (2024).
- [55] D. Barducci, L. Di Luzio, M. Nardecchia, and C. Toni, *J. High Energy Phys.* **12** (2023) 154.
- [56] R. Boto, D. Das, J. C. Romao, I. Saha, and J. P. Silva, *Phys. Rev. D* **109**, 095002 (2024).
- [57] F. Arbabifar, S. Bahrami, and M. Frank, *Phys. Rev. D* **87**, 015020 (2013).
- [58] P. S. Bhupal Dev, D. K. Ghosh, N. Okada, and I. Saha, *J. High Energy Phys.* **03** (2013) 150; **05** (2013) 049.
- [59] E. Ma, *Phys. Lett. B* **772**, 442 (2017).
- [60] in *2001 Europhysics Conference on High Energy Physics* (2001), arXiv:hep-ex/0107031.
- [61] G. Aad *et al.* (ATLAS Collaboration), *Eur. Phys. J. C* **83**, 605 (2023).
- [62] S. Bhattacharya, N. Sahoo, and N. Sahu, *Phys. Rev. D* **96**, 035010 (2017).
- [63] D. López-Val and T. Robens, *Phys. Rev. D* **90**, 114018 (2014).
- [64] T. Robens and T. Stefaniak, *Eur. Phys. J. C* **76**, 268 (2016).
- [65] U. Bellgardt *et al.* (SINDRUM Collaboration), *Nucl. Phys.* **B299**, 1 (1988).
- [66] A. M. Baldini *et al.* (MEG Collaboration), *Eur. Phys. J. C* **76**, 434 (2016).
- [67] E. J. Chun, H. M. Lee, and P. Sharma, *J. High Energy Phys.* **11** (2012) 106.
- [68] G. Aad *et al.* (ATLAS Collaboration), *J. High Energy Phys.* **08** (2022) 104.
- [69] M. A. Shifman, A. I. Vainshtein, M. B. Voloshin, and V. I. Zakharov, *Sov. J. Nucl. Phys.* **30**, 711 (1979).
- [70] A. Djouadi, *Phys. Rep.* **459**, 1 (2008).
- [71] M. Spira, *Fortschr. Phys.* **46**, 203 (1998).
- [72] J. F. Gunion, H. E. Haber, G. L. Kane, and S. Dawson, *The Higgs Hunter’s Guide* (Brookhaven Nat. Lab., Upton, NY, 2000), Vol. 80.
- [73] M. Carena, I. Low, and C. E. M. Wagner, *J. High Energy Phys.* **08** (2012) 060.
- [74] G. Aad *et al.* (ATLAS Collaboration), *J. High Energy Phys.* **07** (2023) 088.
- [75] G. Aad *et al.* (ATLAS Collaboration), *Phys. Lett. B* **809**, 135754 (2020).

- [76] A. M. Sirunyan *et al.* (CMS Collaboration), *J. High Energy Phys.* **07** (2021) 027.
- [77] A. Tumasyan *et al.* (CMS Collaboration), *J. High Energy Phys.* **05** (2023) 233.
- [78] B. W. Lee, C. Quigg, and H. B. Thacker, *Phys. Rev. D* **16**, 1519 (1977).
- [79] M. Aoki and S. Kanemura, *Phys. Rev. D* **77**, 095009 (2008).
- [80] A. G Akeroyd, A. Arhrib, and E. Naimi, *Phys. Lett. B* **490**, 119 (2000).
- [81] D. K. Ghosh, N. Ghosh, I. Saha, and A. Shaw, *Phys. Rev. D* **97**, 115022 (2018).
- [82] G. Belanger, F. Boudjema, A. Pukhov, and A. Semenov, *Comput. Phys. Commun.* **176**, 367 (2007).
- [83] A. Alloul, N. D. Christensen, C. Degrande, C. Duhr, and B. Fuks, *Comput. Phys. Commun.* **185**, 2250 (2014).
- [84] G. Belanger, F. Boudjema, A. Pukhov, and A. Semenov, *Comput. Phys. Commun.* **180**, 747 (2009).
- [85] L. Goodenough and D. Hooper, [arXiv:0910.2998](https://arxiv.org/abs/0910.2998).
- [86] G. Elor, N. L. Rodd, T. R. Slatyer, and W. Xue, *J. Cosmol. Astropart. Phys.* **06** (2016) 024.
- [87] K. S. Babu, S. Chakdar, N. Das, D. K. Ghosh, and P. Ghosh, *J. High Energy Phys.* **07** (2023) 143.
- [88] A. Arhrib, R. Benbrik, M. Chabab, G. Moulataka, and L. Rahili, *J. High Energy Phys.* **04** (2012) 136.
- [89] A. Arhrib, R. Benbrik, M. Chabab, G. Moulataka, M. C. Peyranere, L. Rahili, and J. Ramadan, *Phys. Rev. D* **84**, 095005 (2011).